Time-dependent theory of the Auger resonant Raman effect for diatomic molecules: Concepts and model calculations for N_2 and CO

Zbigniew W. Gortel,[1,*] Robert Teshima,[1] and Dietrich Menzel[2,†]
[1]*Department of Physics, University of Alberta, Edmonton, Alberta, Canada T6G 2J1*
[2]*Physik-Department E20, Technische Universität München, D-85747 Garching, Germany*
(Received 2 February 1998)

We develop an explicitly time-dependent theory for one-step resonant excitation-deexcitation processes of core electron states in diatomic molecules. Emphasis is placed on a conceptual picture demonstrating how the effective time of the formation of the spectra—which is influenced by the bandwidth of the exciting radiation, by the excitation of the molecule being resonant or off resonant (detuned), and by the actual core hole lifetime—changes the appearance of the deexcitation electron spectra. Explicit time-dependent model calculations for three final states each of $1s$-hole excited N_2 (including one spectator decay) and C $1s$–hole excited CO allow demonstration of the various consequences for the spectral shapes which derive from these influences. In particular, off-resonance excitation is shown to shorten the effective time of the spectrum formation below the lifetime of the core-excited state leading to the recently observed collapse of the vibrational structure in the spectrum. Our calculated spectra also demonstrate the influences of the relative positions and shapes of the potential curves involved. On resonance, the nodal structure of the vibrational wave functions of the core-excited state is reflected in the shapes of the spectator decay spectra of N_2 with a soft final state interatomic potential. [S1050-2947(98)05308-6]

PACS number(s): 33.80.Eh, 34.10.+x, 34.50.Gb

I. INTRODUCTION

Excitation and decay of a core hole, whether resonant or nonresonant, are usually considered as two separate steps. This applies to decay via emission of a photon or of an Auger electron. However, when the bandwidth of the exciting radiation is narrower than the core level lifetime width and tuned to the region of a bound resonance, the two-step picture becomes inadequate, and a one-step picture considering the excitation-decay sequence as one coherent process has to be applied. These conditions [1] are usually termed resonant x-ray Raman scattering conditions (when photons are detected), and radiationless resonant Raman scattering or more often Auger resonant Raman effect (ARRE) conditions (when electrons are detected). We are primarily concerned with the latter in this work.

Under such resonant Raman conditions a number of interesting features are found. For ideal resolution of the primary excitation, energy conservation demands that the decay products, whether photons or electrons, contain the surplus energy of the incoming photon when the latter is tuned through a resonance (''linear dispersion''). The linewidths of the decay spectra are not influenced by the lifetime width of the intermediate resonance. The cross section, of course, follows the resonance profile (''resonance enhancement''). Most interestingly, detuning from the resonance leads to distinct changes of the decay spectra. These phenomena have first been seen for decay via photon emission [resonant x-ray scattering (RXS) or emission (RXES)], and more recently in Auger emission (ARRE) as well [2]. The advent of third generation synchrotron radiation sources with high brightness combined with monochromators with high-resolving power has made it possible to perform studies of atomic and molecular decay x-ray and Auger electron emission studies under such conditions with unprecedented detail, and has led to the discovery of very interesting effects [2,3]. In the Auger case and utilizing a nearly (but not ideally) monochromatic source tuned across the lifetime-broadened resonance, the decay spectra have lines which are narrower than the lifetime width of the excited state (e.g., they are narrower than the corresponding normal Auger lines), may be asymmetric or even exhibit a double peak structure, and whose positions and shapes vary, as mentioned above, with the exciting radiation frequency [4–6].

For molecules an additional factor influencing the appearance of the spectra is the presence of lifetime-broadened vibrational structure of the decaying core-excited state and of the vibrational structure of the molecule in the final electronic configuration. Typically, the lifetime broadening of the core-excited state is of the same order as its vibrational level spacing. This leads to effects known as lifetime-vibrational interference in the decay spectra [7–10]. The number of experimental studies under nearly or truly high-resolution core-excitation conditions (ARRE or x-ray emission) rapidly increases for small diatomic molecules like CO [8–13], N_2 [8,14], O_2 [8,15,16], or HCl [17,18], and adsorbed CO [19].

The theoretical treatment of the Auger resonant Raman effect for molecules usually employs a suitably modified Kramers-Heisenberg-type expression [see Eqs. (26) and (27) below] for the Raman scattering amplitude after the nuclear and the electronic degrees of freedom are separated in the Born-Oppenheimer approximation. The x-ray absorption and the electron or x-ray emission events are considered to be a single quantum-mechanical process. The shortcomings of a

*Electronic address: gortel@gortel.phys.ualberta.ca
†Electronic address: menzel@e20.physik.tu-muenchen.de

two-step description in which the emission process is considered to be independent of the x-ray absorption become severe for short living core-excited configurations for which the lifetime-vibrational interference effects become important. Modern derivations of the Kramers-Heisenberg-type expressions use a machinery of many-channel resonant and off-resonant scattering theory [2,20]. These derivations emphasize the time-independent aspects of the problem and make it difficult to obtain direct insight into details of the molecular dynamics in the core-excited state. The resulting expression was used to investigate the dependences of the gross features (like the center of gravity) of the electron and x-ray decay spectra on the radiation frequency and on the radiation spectral distribution for harmonic potential surfaces [21].

Although the explicitly time-independent expression is sufficient to simulate in detail the experimentally observed decay spectra [8–10,13–15], using matrix elements and potential curves which have been obtained by fitting to the experimental data or by first principles calculations [13], detailed insight into the temporal molecular dynamics in the excited state is helpful and often necessary to understand the evolution of the decay spectra as the exciting nearly monochromatic x-ray line is swept across and detuned away from the absorption resonances of the molecule. As examples we mention the electron decay spectra for O_2 [8], the collapse of vibrational structure in decay spectra by frequency detuning in CO [12,22], and the quenching of symmetry breaking in resonant inelastic x-ray scattering by frequency detuning in CO_2 [23–25]. Although a time-independent formalism was used to actually calculate the spectra, the interpretations provided often refer to the time-dependent dynamics in the excited state and introduce the concept of a duration time of the resonant x-ray scattering process [25].

An explicitly time-dependent theory of the nuclear dynamics of decaying states was recently formulated by Cederbaum and Tarantelli [26] who used it to calculate gross features (center of gravity and bandwidth) of the decay spectra for broad (nonmonochromatic) excitation. This approach was then generalized to investigate the effects of the competition between narrow-band core excitation and electronic decay on ARRE [27], and on radiative and nonradiative x-ray resonant scattering spectra [24,28]. In particular, in Ref. [27] the ARRE spectra were computed for N_2 and O_2 molecules within the time-independent approach and compared with the ones calculated by numerically solving a set of coupled time-dependent Schrödinger equations. The latter approach has the advantage that it is possible to observe how the spectra are formed as the system evolves in time. However, it is CPU-time intensive and the interpretational appeal of an analytic derivation of explicitly time-dependent expressions for the spectra from these equations is lost. We have already applied in the past [29] the time-dependent approach used in this work to investigate vibrationally resolved photodissociation of diatomic molecules through the Auger decay of a bonding core-excited state and Sec. II may be viewed also to be a derivation of the expressions used there.

In carrying through the development of our own approach in addition to the existing treatments mentioned, we have been motivated by the following three goals. First, aiming at the reader not mainly interested in purely theoretical aspects of ARRE, but rather in the ability to relate the observed features of the spectra to the time evolution of the system in the metastable excited state, we derive an explicitly time-dependent expression for the Auger resonant Raman cross section following the explicitly time-dependent formalism. The derivation, although lengthy, is simple: we start from the time-dependent Schrödinger equation for a coupled electron-nuclei system, decouple it using the Born-Oppenheimer approximation, and solve the resulting set of coupled differential equations using plausible approximations along the way. The result could be as well derived from the Kramers-Heisenberg-type expression for the Raman scattering amplitude. Nevertheless, we choose to present the complete, explicitly time-dependent derivation to emphasize the role played by the molecular femtosecond dynamics of the molecule in the metastable excited state in the formation process of the Auger electron decay spectra under different tuning conditions of the incident nearly monochromatic x-ray radiation. The concept of effective lifetime, i.e., the duration time of the scattering process, appears in this approach quite naturally. Secondly, we want to demonstrate that the time-dependent expression for the cross section is not only intuitively attractive but that it is also a practical tool allowing us to calculate the spectra. We do this by calculating the ARRE spectra for two participant and one spectator decay of core-excited N_2 and three participant decays of C $1s$–hole core-excited CO using Morse potential parametrizations of all intramolecular potentials involved, and following the time evolution of the system numerically. Thirdly, we want to relate the evolution of the spectra (i.e., their peak positions, numbers of peaks, and their shapes) to the effective duration of the system evolution in the metastable core-excited state, which changes as the incoming x-ray radiation is swept through and away from the vibrational resonances. As mentioned above, this point was already made in the most recent literature on the subject, but in our time-dependent approach it can be demonstrated explicitly.

The outline of the paper is as follows. The theoretical derivation is presented in Sec. II along with the discussion of the qualitative features of the expected spectra. Certain more technical points are found in Appendixes A and B. Section III is devoted to the numerical calculation of the spectra and a detailed discussion of their features. This is mainly done for N_2, with CO serving to strengthen the points already made for N_2, and to emphasize some additional ones. Analytic expressions for all the wave functions used in this part are listed in Appendix C. A short summary and conclusions are contained in Sec. IV.

Before proceeding, several points should be stressed. First, all numerical results presented in this paper could as well be obtained (and some of them were, indeed [9,10,13–15]) in the time-independent approaches. In particular, the lifetime-vibrational interference effects discussed in these references are fully accounted for in our examples although, in our opinion, the explicit decomposition of the spectra into ''direct'' and ''interference'' contributions [cf. Eqs. (26) and (27) below] emphasized in these works is a somewhat artificial result of the time-independent approach. Less numerical effort is needed in our time-dependent approach, particularly for systems with shorter lifetimes. Second, the time-independent approach becomes numerically impractical, at

least without further approximations, for systems with dissociating excited states [18,28,30] while our time-dependent expressions can be evaluated in such cases without any added numerical effort. Third, for such systems, and probably for adsorbed species as well, a dependence of the Auger decay rate on nuclear coordinate should be accounted for. For time-independent approaches (which must be reformulated right from the start) this would result in almost intractable numerics [31] while the time-dependent expression, trivially modified, may be a starting point for numerical calculations which can be handled by the programs developed in the course of this work. Work in this direction is in progress. Fourth, the time-dependent expressions for the electron spectra can be further simplified. For example, the time evolution in the core-excited state can be followed analytically for harmonic representation of the corresponding potential surface. Even for the Morse potential representation, an approximate analytic time evolution can be given [32,33] based on Heller's [34] semiclassical method. Not much is gained in such cases when the time-independent approach is used.

II. THEORY

In this section we develop the one-step theory of resonant core excitation followed by Auger decay for molecules under conditions of narrow-band primary excitation, i.e., below the lifetime width of the intermediate core-excited state. These conditions are usually termed Auger resonant Raman conditions and, as mentioned, can be realized experimentally by utilization of third generation synchrotron radiation (SR) sources. We will explicitly use a time-dependent approach to the nuclear dynamics not only because it is numerically more efficient than its time-independent counterpart but also because it provides intuitive and physically attractive interpretations of the main features of the numerical results. Although our initial theoretical formulation, analogous to the approach proposed to model Raman scattering [35], is quite general, the theory will be applied specifically to diatomic molecules for which the nuclear dynamics is essentially one dimensional. For the sake of completeness and to strengthen the interpretative and pedagogical aspects of our approach, we provide in Secs. II A and II B an explicit time-dependent derivation of the spectra with all approximations explicitly spelled out. The reader interested mainly in the results and their interpretation may take note of Eq. (22) and the discussion following it, and then proceed directly to Sec. II D.

A. Basic equations and their solutions

Consider a molecule as a physical system consisting of nuclei and electrons interacting with the soft x-ray radiation. We denote a collection of coordinates specifying nuclear positions by $\boldsymbol{r}$ and those of all electrons by x. For a diatomic molecule $\boldsymbol{r}$ is a vector joining the two nuclei. The total Hamiltonian of the system $\hat{H}(\boldsymbol{r},x)$ can, in the spirit of the Born-Oppenheimer approach, be written as a sum

$$\hat{H}=T+H_e-\boldsymbol{\mu}\cdot\boldsymbol{\mathcal{E}}(t). \tag{1}$$

The kinetic nuclear energy T involves derivatives with respect to the nuclear coordinates $\boldsymbol{r}$. The ''electronic Hamiltonian'' $H_e(\boldsymbol{r},x)$ depends parametrically on $\boldsymbol{r}$ and consists of the kinetic energies of all electrons, and of electron-electron, electron-nuclei, and nuclei-nuclei potential interactions. In the dipole approximation the interaction with the radiation field involves the molecular dipole moment $\boldsymbol{\mu}(\boldsymbol{r},x)$ and the radiation electric field $\boldsymbol{\mathcal{E}}(t)=\boldsymbol{\mathcal{E}}_0(\omega)\cos(\omega t)$. Initially, for $t<0$, i.e., before the molecule gets illuminated by the radiation field, the system is in the global (i.e., electronic and nuclear) ground state of the molecule $|\Psi_{\rm in})\rangle$ which then evolves according to the Schrödinger equation

$$\hat{H}|\Psi(t))\rangle=i\hbar\frac{d}{dt}|\Psi(t))\rangle. \tag{2}$$

Here, we use Dirac's notation: a ''double'' ket $|\ldots)\rangle$ is used to represent electronic, $|\ldots)$, and nuclear, $|\ldots\rangle$, degrees of freedom, respectively. The subscript ''in'' stands for ''initial'' throughout the entire paper.

To proceed with the solution of Eq. (2) we identify state vectors of diabatic electronic configurations relevant to the process considered. Thus we have the ground state configuration $|\Phi_g)$ with all electrons filling the lowest-energy orbitals. The radiation excites the system resonantly to a configuration in which an electron is promoted from an atomic core orbital (usually the $1s$ orbital of one of the atoms) to the lowest unoccupied molecular orbital. We denote by $|\Phi_d)$ the corresponding core-excited state. This configuration is unstable against Auger autoionization decay in which one of the outer shell electrons fills the core hole and another is released from the molecule. The electron promoted in the preceding excitation step may or may not participate in the decay giving rise to the commonly used distinction between ''participant'' and ''spectator'' Auger decay process. If $\boldsymbol{k}$ is the set of all quantum numbers needed to identify the quantum state of the released electron (if spin is ignored then $\hbar\boldsymbol{k}$ is the free electron momentum) and f identifies the final electronic configuration of the ionic molecule, then we denote by $|\Phi_{f\boldsymbol{k}})$ the state of the corresponding final electronic configuration. The outgoing electron is included in it, so we have an entire continuum of possible final electronic configurations corresponding to the continuum of states of the released electron. The subscripts g, d, and f in the state vectors above and in the corresponding quantities defined later stand for ''ground,'' ''discrete'' (core-excited state), and ''final (ionic)'' electronic configurations. Different Auger decays correspond to different final ionic configurations f. In the spirit of the Born-Oppenheimer approximation all the state vectors defined above depend parametrically on the actual value of the nuclear coordinates $\boldsymbol{r}$.

Expanding the global state vector $|\Psi(t))\rangle$ into these electronic configurations

$$|\Psi(t))\rangle=|\chi_g(t)\rangle\,|\Phi_g)+|\chi_d(t)\rangle\,|\Phi_d)+\sum_{f,\boldsymbol{k}}|\chi_{f\boldsymbol{k}}(t)\rangle\,|\Phi_{f\boldsymbol{k}}), \tag{3}$$

inserting it into the Schrödinger equation (2), and closing from the left with $(\Phi_\alpha|$ ($\alpha=g,d$, and $(f\boldsymbol{k})$) we obtain the set of coupled equations (which, for the sake of brevity, will not be given here) for the ''expansion coefficients'' $|\chi_\alpha(t)\rangle$. In the position representation these coefficients depend on the

nuclear coordinates $\boldsymbol{r}$ and are the wave functions describing the state of the nuclear motion when the electrons are in the αth configuration. Deriving these equations, the Born-Oppenheimer approximation is used, i.e., the contributions due to the action of the kinetic energy operator T on the electronic states $|\Phi_\alpha\rangle$ are ignored. Furthermore, it is assumed that the states describing the electronic configurations are chosen in such a way that only the following matrix elements of the Hamiltonian do not vanish:

$$(\Phi_g|H_e|\Phi_g)=V_g, \tag{4a}$$

$$(\Phi_d|H_e|\Phi_d)=V_d, \tag{4b}$$

$$(\Phi_{f\boldsymbol{k}}|H_e|\Phi_{f\boldsymbol{k}})=V_{f\boldsymbol{k}}\equiv V_f+\mathcal{E}_{\boldsymbol{k}}, \tag{4c}$$

$$(\Phi_d|H_e|\Phi_{f\boldsymbol{k}})=W_{f\boldsymbol{k}}, \tag{4d}$$

$$(\Phi_d|\boldsymbol{\mu}|\Phi_g)\cdot\boldsymbol{\mathcal{E}}(t)=\boldsymbol{D}\cdot\boldsymbol{\mathcal{E}}(t). \tag{4e}$$

Diagonal matrix elements of H_e, i.e., V_g, V_d, and $V_{f\boldsymbol{k}}$ are the $\boldsymbol{r}$-dependent energies of the system of all electrons in the corresponding electronic configurations. Note, however, that due to the negligible influence of the released electron on the energy of the electrons remaining with the molecule, the energy $V_{f\boldsymbol{k}}$ is the sum of the kinetic energy of the released electron $\mathcal{E}_{\boldsymbol{k}}$ and the $\boldsymbol{r}$-dependent energy V_f of the electrons remaining with the molecular ion. The only nonvanishing off-diagonal element of H_e [Eq. (4d)] represents the Auger autoionizing coupling between the discrete core-excited molecular configuration d and the continuum of final electronic ionic configurations $(f\boldsymbol{k})$: the electronic level V_d is embedded within the continuum of $V_{f\boldsymbol{k}}$ levels. Finally, it is assumed that the molecular dipole moment couples only the ground state configuration g with the core-excited configuration d. The possibility of direct photoemission [i.e., dipole coupling between g and $(f\boldsymbol{k})$ configurations] is, therefore, ignored here. Our present treatment is thus not appropriate for the discussion of interference effects between direct and resonant photoemission. It can be generalized to include these effects without too much effort. For future use it is convenient to define the molecular Hamiltonians

$$H_\alpha=T+V_\alpha, \tag{5}$$

where $\alpha=g,d$, and f. At $t=0$ all $|\chi_\alpha(t=0)\rangle$ vanish except for the ground state electronic configuration $(\alpha=g)$ for which the initial condition is

$$|\chi_g(t=0)\rangle=|\psi_{\rm in}\rangle, \tag{6}$$

where $|\psi_{\rm in}\rangle$ is the ground state wave vector of the electronic ground state Hamiltonian H_g. The energy eigenvalue corresponding to it, $E_{\rm in}$, is the lowest possible energy of the system.

For sufficiently weak interaction with the electromagnetic radiation we may expand the solutions $|\chi_\alpha(t)\rangle$ into a power series in the strength of the radiation field and keep only the contributions independent of it, $|\chi_\alpha^{(0)}(t)\rangle$, and the contributions linear in it, $|\chi_\alpha^{(1)}(t)\rangle$. Correspondingly, the equations break down into a set independent of the field and another set linear in it. Solving the first set leads to $|\chi_\alpha^{(0)}(t)\rangle=0$ for $\alpha=d$ and $(f\boldsymbol{k})$ because the radiation field is needed to promote the system to these configurations. For $|\chi_g^{(0)}(t)\rangle$ one gets the stationary state evolution $\exp(-iE_{\rm in}t/\hbar)|\psi_{\rm in}\rangle$. Next, the set of equations for the contributions linear in the field is obtained

$$i\hbar\frac{d}{dt}|\chi_d(t)\rangle=H_d|\chi_d(t)\rangle+\sum_{f,\boldsymbol{k}}W_{f\boldsymbol{k}}|\chi_{f\boldsymbol{k}}(t)\rangle - e^{-(i/\hbar)E_{\rm in}t}\boldsymbol{\mathcal{E}}(t)\cdot\boldsymbol{D}|\psi_{\rm in}\rangle, \tag{7a}$$

$$i\hbar\frac{d}{dt}|\chi_{f\boldsymbol{k}}(t)\rangle=(H_f+\mathcal{E}_{\boldsymbol{k}})|\chi_{f\boldsymbol{k}}(t)\rangle+W_{f\boldsymbol{k}}^\dagger|\chi_d(t)\rangle, \tag{7b}$$

subjected to the initial conditions $|\chi_d(t=0)\rangle=|\chi_{f\boldsymbol{k}}(t=0)\rangle=0$. There is one equation like Eq. (7b) for each possible Auger decay mode f. The superfluous superscript (1) is dropped in Eqs. (7). These equations differ from the usual Schrödinger equations by the presence of the core hole–ionic coupling terms defined in Eq. (4d). Furthermore, the radiation field continuously promotes the system from the initial ground state configuration $|\psi_{\rm in}\rangle$ up to the core-excited state [cf. the last term in Eq. (7a)]. The set of Eqs. (7) should be solved for $|\chi_{f\boldsymbol{k}}(t)\rangle$ which describes the state of the nuclear motion of the molecular ion in the final state f at a time t provided that the departing Auger electron has a momentum $\hbar\boldsymbol{k}$.

Formally, a solution to Eq. (7b) is

$$|\chi_{f\boldsymbol{k}}(t)\rangle=(i\hbar)^{-1}\int_0^t dt' e^{-(i/\hbar)(H_f+\mathcal{E}_{\boldsymbol{k}})(t-t')}W_{f\boldsymbol{k}}^\dagger|\chi_d(t')\rangle. \tag{8}$$

Inserted into Eq. (7a) it gives

$$i\hbar\frac{d}{dt}|\chi_d(t)\rangle=H_d|\chi_d(t)\rangle+(i\hbar)^{-1}\times\int_0^t dt'\,\mathcal{F}(t')|\chi_d(t-t')\rangle - e^{-(i/\hbar)E_{\rm in}t}\boldsymbol{\mathcal{E}}(t)\cdot\boldsymbol{D}|\psi_{\rm in}\rangle, \tag{9}$$

where the second term on the right-hand side accounts for the memory of the entire past evolution of $|\chi_d(t)\rangle$ through the memory kernel

$$\mathcal{F}(t)=\sum_{f,\boldsymbol{k}}W_{f\boldsymbol{k}}\,e^{-(i/\hbar)(H_f+\mathcal{E}_{\boldsymbol{k}})t}\,W_{f\boldsymbol{k}}^\dagger. \tag{10}$$

Physically, reading Eq. (8) from right to left, the system evolves first in the core-excited electronic configuration d up to time t' when it decays emitting an electron with momentum $\hbar\boldsymbol{k}$ (term $W_{f\boldsymbol{k}}^\dagger$). Then, the system evolves up to time t along the potential energy surface V_f (recall that H_f in the exponential time evolution operator contains V_f). The time integration accounts for the fact that the decay may occur at any instant between 0 and t. The time evolution in the core-excited electronic configuration d, as given by Eq. (9), is more complicated as it is affected not only by the usual evolution along the potential energy surface V_d (contained in

H_d) and by the continuous radiation pumping from the ground state but, as seen in Eq. (10), also by virtual transitions from the core-excited configuration to an ionic one [term $W^{\dagger}_{f\boldsymbol{k}}$ in Eq. (10)], followed by the evolution along V_f and then by the virtual transition back to the core-excited configuration. The summation over f in Eq. (10) is due to the fact that virtual transitions may occur ''to'' and ''back from'' any ionic configuration f.

To deal with the memory kernel we note that the summation over $\boldsymbol{k}$ in Eq. (10) is in fact an integration over the broad free electron energy spectrum because each $W_{f\boldsymbol{k}}$ is expected to vary slowly across the spectrum. Therefore we assume that $W_{f\boldsymbol{k}}=W_f$ does not depend on $\boldsymbol{k}$ at all and convert the summation over $\boldsymbol{k}$ into the integration over $\mathcal{E}_{\boldsymbol{k}}$. The expression on the right-hand side of Eq. (10) becomes proportional to $\delta(t)$, i.e., effectively the memory in the system is wiped out. The result is

$$\mathcal{F}(t)\approx\pi\hbar\rho_e\sum_f |W_f|^2\delta(t)=\frac{\hbar}{2}\Gamma\delta(t), \tag{11}$$

where $\Gamma=2\pi\rho_e\Sigma_f|W_f|^2$ and ρ_e is the average value of the free electron density of states over the relevant part of the free electron spectrum. Inserting now Eq. (11) into Eq. (9) we get

$$i\hbar\frac{d}{dt}|\chi_d(t)\rangle=\left(H_d-\frac{i}{2}\Gamma\right)|\chi_d(t)\rangle-e^{-(i/\hbar)E_{\rm in}t}\boldsymbol{\mathcal{E}}(t)\cdot\boldsymbol{D}|\psi_{\rm in}\rangle, \tag{12}$$

which apart from the last radiation pumping term looks like an ordinary time-dependent Schrödinger equation in which an imaginary optical potential $-i\Gamma(\boldsymbol{r})/2$ is added to the potential energy $V_d(\boldsymbol{r})$. Its presence accounts for all possible Auger decays and results in the gradual decrease of the amplitude of $|\chi_d(t)\rangle$ with time.

Usually, more than one decay Auger mode is available for the decay of the core-excited state. This is taken into account by summing over f in the middle term on the right-hand side of Eq. (7a) and by having one equation like Eq. (7b) for each possible decay mode f. The optical potential Γ in Eq. (12) is due to all possible modes of Auger decay and it appears in Eq. (8) implicitly through $|\chi_d(t)\rangle$. $W^{\dagger}_{f\boldsymbol{k}}$ explicitly present in Eq. (8) refers, however, to the individual-mode decay rate corresponding to the particular final electronic configuration f to which the state vector $|\chi_{f\boldsymbol{k}}(t)\rangle$ belongs.

Two more approximations will be made in what follows. In contrast, however, to the approximation in which the memory effects are ignored, they may be relatively easily relaxed in a more sophisticated version of the theory. The first one replaces the $\boldsymbol{r}$-dependent optical potential Γ with a coordinate-independent constant. This approximation might, however, be questionable for systems in which the core-excited state is purely repulsive along some generalized coordinate. This is because the Auger decay rate in a molecular configuration (when all constituents of the molecule are close together) may be different from the Auger decay rate when one atom (or group of atoms) gets substantially separated from the rest. In the second approximation we assume that the transition dipole moment $\boldsymbol{D}$, defined in Eq. (4e), does not depend on the nuclear coordinates $\boldsymbol{r}$, in particular that it does not depend on the orientation of the molecule. This approximation allows us later on to pull out $\boldsymbol{\mathcal{E}}(t)\cdot\boldsymbol{D}$ in front of all operators but it precludes a correct treatment of the dependence of the investigated processes on the polarization of the incoming radiation.

Invoking both approximations in Eq. (12) one can check by direct substitution that its solution is

$$|\chi_d(t)\rangle=-(i\hbar)^{-1}\boldsymbol{\mathcal{E}}_0(\omega)\cdot\boldsymbol{D}\int_0^t dt' e^{-(i/\hbar)E_{\rm in}(t-t')}\times\cos[\omega(t-t')]e^{-\Gamma t'/2\hbar}|\phi_d(t')\rangle. \tag{13}$$

Here, $|\phi_d(t)\rangle$ is the solution of a standard time-dependent Schrödinger equation without the optical potential and without the radiation driven term

$$i\hbar\frac{d}{dt}|\phi_d(t)\rangle=H_d|\phi_d(t)\rangle, \tag{14}$$

subjected to the initial condition $|\phi_d(t=0)\rangle=|\psi_{\rm in}\rangle$. The explicit time dependence of the radiation field was used in Eq. (13).

Equations (8) and (13) together form an approximate solution to Eqs. (7). For these solutions to be of use a standard time-dependent Schrödinger equation (14) must be independently solved. In the next section these solutions will be used to derive quantities of direct experimental interest.

B. Observables

Note that the final electronic configuration corresponds to a free electron receding with a momentum $\hbar\boldsymbol{k}$ from the molecular ion in the electronic configuration f whose internal molecular motion is governed by the Hamiltonian H_f. Using a properly designed detector the ion may be detected in any eigenstate of H_f:

$$H_f|\varphi^f_\chi\rangle=E^f_\chi|\varphi^f_\chi\rangle. \tag{15}$$

Here, χ represents the set of all quantum numbers necessary to identify the eigenstate of the nuclear motion in which the molecular ion can be detected. In particular, such a state may belong to either a discrete (vibrationally excited molecular ion, localized states) or a continuous (dissociating ion, extended states) spectrum of H_f. The superscripts f are used in Eq. (15) to specify the electronic configuration of the molecular ion after decay, i.e., it specifies a particular Auger decay mode. When a molecule is illuminated by radiation in the frequency interval $(\omega,\omega+d\omega)$ then

$$d\dot{P}_{\chi,f\boldsymbol{k}}(\omega)=\lim_{t\to\infty}\frac{d}{dt}|\langle\varphi^f_\chi|\chi_{f\boldsymbol{k}}(t)\rangle|^2 \tag{16}$$

is the rate (probability per unit time) that the released electron having momentum $\hbar\boldsymbol{k}$ (and energy $\mathcal{E}_{\boldsymbol{k}}$) leaves behind a molecular ion in the state χ of its nuclear motion due to the fth mode of Auger decay. The differential in $d\dot{P}$ refers to the frequency interval $d\omega$, i.e., we anticipate here that $d\dot{P}$ is proportional to $d\omega$. The rate with which the ions in the fth electronic configuration and χth state of their internal motion

are generated, and the rate with which the Auger electrons with a momentum $\hbar\boldsymbol{k}$ and resulting from fth mode of decay are detected are, respectively,

$$d\dot{P}_{\chi,f}(\omega)=\sum_{\boldsymbol{k}} d\dot{P}_{\chi,f\boldsymbol{k}}(\omega), \tag{17a}$$

$$d\dot{P}_{f\boldsymbol{k}}(\omega)=\sum_{\chi} d\dot{P}_{\chi,f\boldsymbol{k}}(\omega). \tag{17b}$$

The rate in Eq. (17a) for χ restricted to the dissociating extended states of H_f was recently used [29] to investigate the photon energy-dependent photodissociation yield and the N^+ time of flight spectra for the core hole photoexcited N_2 molecules. In this work we concentrate on the Auger electron spectra which will now be derived from the rate in Eq. (17b).

To get the matrix element needed in Eq. (16) we insert $|\chi_d(t)\rangle$ given in Eq. (13) into Eq. (8) to get $|\chi_{f\boldsymbol{k}}(t)\rangle$. We close it from the left with $\langle\varphi_\chi^f|$, use Eq. (15) to replace H_f with E_χ^f in the exponent, and replace $\cos[\omega(t-t')]$ with a sum of exponentials. After dropping the irrelevant time-dependent overall phase factor we get

$$\begin{aligned}\langle\varphi_\chi^f|\chi_{f\boldsymbol{k}}(t)\rangle &= -(i\hbar)^{-2}\frac{1}{2}\boldsymbol{\mathcal{E}}_0(\omega)\cdot\boldsymbol{D}\Bigg\{\int_0^t dt' e^{-(i/\hbar)(E_{\rm in}+\hbar\omega-E_\chi^f-\mathcal{E}_{\boldsymbol{k}})t'}\\ &\times\int_0^{t'} dt'' e^{(i/\hbar)(E_{\rm in}+\hbar\omega)t''}\\ &\times e^{-\Gamma t''/2\hbar}\langle\varphi_\chi^f|W_{f\boldsymbol{k}}^\dagger|\phi_d(t'')\rangle\\ &+\int_0^t dt' e^{-(i/\hbar)(E_{\rm in}-\hbar\omega-E_\chi^f-\mathcal{E}_{\boldsymbol{k}})t'}\\ &\times\int_0^{t'} dt'' e^{(i/\hbar)(E_{\rm in}-\hbar\omega)t''}\\ &\times e^{-\Gamma t''/2\hbar}\langle\varphi_\chi^f|W_{f\boldsymbol{k}}^\dagger|\phi_d(t'')\rangle\Bigg\}.\end{aligned} \tag{18}$$

As already noted, $\boldsymbol{D}$ was pulled out to the left of all operators. If its $\boldsymbol{r}$ dependence would have to be accounted for, then $\boldsymbol{D}$ should be placed inside the matrix element to the right of $W_{f\boldsymbol{k}}^\dagger$. The two terms in the curly brackets differ only in sign in front of $\hbar\omega$.

According to Eq. (16), the above matrix element must be squared and differentiated with respect to t before the limit $t\to\infty$ is taken. The procedure is of some interest but rather technical so the details are given in Appendix A. The net result is that, if $E_{\rm in}$ is the lowest energy which the system can have, then only the first term in the curly brackets of Eq. (18) contributes. In the long-time limit, this gives an expression for $d\dot{P}_{\chi,f\boldsymbol{k}}(\omega)$ which is proportional to $\delta(E_{\rm in}+\hbar\omega-E_\chi^f-\mathcal{E}_{\boldsymbol{k}})$. The latter expresses the overall energy conservation for the process. Squaring the matrix element we encounter a square of the electric field amplitude $\mathcal{E}_0(\omega)$ which can be related to the radiation intensity $dI(\omega)$ within the frequency interval $\omega,\omega+d\omega$:

$$[\mathcal{E}_0(\omega)]^2=\left[\frac{1}{4\pi\epsilon_0}\right]\frac{8\pi}{c}dI(\omega)=\left[\frac{1}{4\pi\epsilon_0}\right]\frac{8\pi}{c}I_0G(\omega-\omega_L)d\omega, \tag{19}$$

where I_0 is the total radiation intensity, $G(\omega-\omega_L)$ is the radiation line shape function centered around the nominal radiation frequency ω_L, and c is the speed of light in vacuum. The factor in the square brackets containing the vacuum permittivity constant ϵ_0 should be ignored if the Gaussian system of units is used. For radiation with a Gaussian line shape with full width at half maximum (FWHM) equal to Γ_L we have

$$G(\omega-\omega_L)=\left(\frac{2\ln 4}{\pi\Gamma_L^2}\right)^{1/2}\exp[-2\ln 4(\omega-\omega_L)^2/\Gamma_L^2]. \tag{20}$$

As anticipated below Eq. (16), $d\dot{P}_{\chi,f\boldsymbol{k}}(\omega)$ is proportional to $d\omega$ and the probability per unit time that a molecule illuminated by the beam of intensity I_0 and a nominal frequency ω_L emits in the fth Auger decay mode an electron with a momentum $\hbar\boldsymbol{k}$ is

$$\begin{aligned}\dot{P}_{f\boldsymbol{k}}(\omega_L)\equiv\int d\dot{P}_{f\boldsymbol{k}}(\omega)&=\left[\frac{1}{4\pi\epsilon_0}\right]\frac{4\pi^2}{c\hbar^4}I_0D^2|W_f|^2\\ &\times\sum_\chi G((E_\chi^f+\mathcal{E}_{\boldsymbol{k}}-E_{\rm in}-\hbar\omega_L)/\hbar)\\ &\times\left|\int_0^\infty dt e^{(i/\hbar)(E_\chi^f+\mathcal{E}_{\boldsymbol{k}})t}\,e^{-\Gamma t/2\hbar}\langle\varphi_\chi^f|\phi_d(t)\rangle\right|^2.\end{aligned} \tag{21}$$

Here, D is the projection of $\boldsymbol{D}$ on the direction of the electric field, and the Auger decay matrix element $W_{f\boldsymbol{k}}^\dagger$ was replaced with a constant W_f and pulled outside the matrix element in Eq. (18). Note that W_f in front of the above expression corresponds to the *particular* Auger decay mode corresponding to the final electronic configuration f of the ion, in contrast to the $\Sigma_f|W_f|^2$ defining the decay rate Γ [cf. Eq. (11) and the discussion after Eq. (12)]. The energy conservation Dirac δ function was effectively replaced with the line profile Gaussian when the integration across the spectral line was made. Note that $\dot{P}_{f\boldsymbol{k}}(\omega_L)$ contains $\boldsymbol{k}$ through $\mathcal{E}_{\boldsymbol{k}}$ so it does not depend on the direction of $\boldsymbol{k}$. This behavior is expected for randomly oriented molecules in a gas and/or unpolarized radiation but here it results from neglecting a possible $\boldsymbol{r}$ dependence of $\boldsymbol{D}$ and is obtained *before* any averaging over molecular orientations and/or polarization was done. This makes such averaging unnecessary, and the comparison of our results should be made with averaged experimental results.

So far $\boldsymbol{k}$ is a discrete index and in order to convert the probabilities into probability distributions, appropriate density of state factors must be introduced. Thus $\dot{P}_{f\boldsymbol{k}}(\omega_L)\rho_e(\mathcal{E})d\mathcal{E}d\Omega/4\pi$ is a probability per unit time that an irradiated molecule emits an electron within the energy interval $(\mathcal{E},\mathcal{E}+d\mathcal{E})$ into a solid angle $d\Omega$ (in an arbitrary direction). Writing down this expression explicitly, one should

replace $\mathcal{E}_{\boldsymbol{k}}$ with $\mathcal{E}$. Dividing further by the flux of the incident photons $I_0/\hbar\omega_L$ and by $d\mathcal{E}d\Omega$ we arrive at the electron energy-dependent differential cross section for the electron emission process. Among others, it contains a factor $2\pi\rho_e(\mathcal{E})|W_f|^2$ which, being proportional to $\sqrt{\mathcal{E}}$, is practically constant because typical Auger electron energies are of the order of a few hundred eV, while an Auger spectrum for any decay mode extends only over a few eV. Therefore, consistently with the definition below Eq. (11), this factor may be replaced with the decay constant Γ_f being a contribution which the particular fth Auger decay mode brings to the overall decay rate Γ. Thus we get the following expression for the differential cross section:

$$\frac{d^2\sigma_e(\mathcal{E})}{d\mathcal{E}d\Omega}=\left[\frac{1}{4\pi\epsilon_0}\right]\frac{\Gamma_f\omega_L D^2}{2c\hbar^3}\times\sum_{\chi} G((E_\chi^f+\mathcal{E}-E_{\rm in}-\hbar\omega_L)/\hbar)\times\left|\int_0^\infty dt e^{(i/\hbar)(E_\chi^f+\mathcal{E})t}\, e^{-\Gamma t/2\hbar}\langle\varphi_\chi^f|\phi_d(t)\rangle\right|^2. \tag{22}$$

Recall that the summation over χ is a summation over all possible eigenstates, localized and extended ones, of the Hamiltonian H_f. Normalization in a box of volume V is used for the extended states so the quantum index χ is discrete and $\langle\varphi_\chi^f|\varphi_{\chi'}^f\rangle=\delta_{\chi,\chi'}$.

A simple property of the time integral in Eq. (22) will be useful in the ensuing discussion of the electron spectra. If in the integral

$$\int_0^\infty dt e^{(i/\hbar)\Omega t}\, e^{-\Gamma t/2\hbar}F(t), \tag{23}$$

the function $F(t)$ varies slowly in time in comparison with the exponential factors then the main contribution to the integral is due to times limited by the *effective lifetime* $\tau_{\rm eff}=2\hbar/\Gamma_{\rm eff}$, where

$$\Gamma_{\rm eff}/2=\sqrt{\Omega^2+(\Gamma/2)^2}. \tag{24}$$

Consequently, the time spans over which the integrand in Eq. (22) effectively contributes to the formation of the electron spectrum may, for certain energies $\mathcal{E}$, be significantly shortened below the actual lifetime $2\hbar/\Gamma$ by the destructive oscillations in the time of the integrand in Eq. (21). An effective lifetime, called the duration time of the resonant x-ray scattering process, was recently introduced in Ref. [25] and used to account for the collapse of vibrational structure in decay spectra by frequency detuning in CO [12,22], and for quenching of symmetry breaking in resonant inelastic x-ray scattering by frequency detuning in CO_2 [23–25].

We conclude with relating the time-dependent result for the cross section to the normally used Kramers-Heisenberg-type expression derived within the time-independent approach. We introduce the eigenstates of the core-excited state Hamiltonian H_d, i.e., $|\psi_v^d\rangle$ corresponding to the energy eigenvalues E_v^d. The quantum number v stands for all quantum numbers needed to specify the vibrational state of the core-excited molecule and it is assumed here that the dissociating states of such a molecule have negligible overlap with the initial state $|\psi_{\rm in}\rangle$, i.e., the core hole excitation does not lead directly to dissociation. The solution of the Schrödinger equation (14) can be written as

$$|\phi_d(t)\rangle=\sum_v \exp\left(-\frac{i}{\hbar}E_v^d t\right)|\psi_v^d\rangle\langle\psi_v^d|\psi_{\rm in}\rangle, \tag{25}$$

and inserted into Eq. (22). We note in passing that this assumption *is not* made in our time-dependent approach here. This will allow us to apply it to the treatment of weakly bounding or dissociating core-excited states without any additional numerical effort. The time integration in Eq. (22) can then be explicitly performed and the resulting cross section is

$$\frac{d^2\sigma_e(\mathcal{E})}{d\mathcal{E}d\Omega}=\left[\frac{1}{4\pi\epsilon_0}\right]\frac{\omega_L D^2}{c\hbar}\sum_{\chi} G((E_\chi^f+\mathcal{E}-E_{\rm in}-\hbar\omega_L)/\hbar)\times(M_{\rm dir}+M_{\rm int}), \tag{26}$$

where

$$M_{\rm dir}=\sum_v |\langle\varphi_\chi^f|\psi_v^d\rangle\langle\psi_v^d|\psi_{\rm in}\rangle|^2\frac{\Gamma_f/2}{(E_\chi^f+\mathcal{E}-E_v^d)^2+(\Gamma/2)^2}, \tag{27a}$$

$$M_{\rm int}=\sum_{v,v'}^{v\neq v'}\langle\psi_{\rm in}|\psi_v^d\rangle\langle\psi_v^d|\varphi_\chi^f\rangle\langle\varphi_\chi^f|\psi_{v'}^d\rangle\langle\psi_{v'}^d|\psi_{\rm in}\rangle\times\frac{\Gamma_f/2}{(E_\chi^f+\mathcal{E}-E_v^d-i\Gamma/2)(E_\chi^f+\mathcal{E}-E_{v'}^d+i\Gamma/2)} \tag{27b}$$

are sometimes referred to as *direct* and *interference* terms [36], respectively. The direct term contains a series of Lorentzian peaks of FWHM determined by the lifetime of the core-excited state and centered around the electron energy $\mathcal{E}$ equal to the energy difference between the vibrational energy E_v^d of the core-excited molecule and the final internal energy E_χ^f of the molecular ion. The interference term was investigated in detail by Gel'mukhanov *et al.* [37]. If the interference term is ignored, the Auger spectrum is a product of the Lorentzians with the spectral line Gaussian $G(\omega-\omega_L)$ given in Eq. (20). This was anticipated in a recent analysis of the atomic ARRE [4,5]. The interference term contributes to the spectra in the wings of the peaks given by the direct term and is responsible for the lifetime-interference effects in Auger emission spectra of molecules [8–10]. In our view the division of the spectra into direct and interference terms is a somewhat artificial result of the more commonly used time-independent picture of the process. Such a distinction is absent from the time-dependent picture.

Usually the time-independent treatment has been applied for numerical analysis and interpretation of Auger and x-ray scattering spectra [8,9,13,15,23,36] although the time-dependent picture has also been invoked in a qualitative [12,18,21,22,28] analysis. In Ref. [27] the time-dependent

approach was explicitly used for the quantitative analysis by directly solving Eqs. (7b) and (12) numerically. This approach allows one to follow the formation of the Auger electron spectra in time as the wave packet evolves along the core-excited state potential surface. The same insight can, however, be gained by calculating the spectra from Eq. (22) for several lifetimes $\hbar/\Gamma$ or, as we will see later, for the x-ray radiation significantly detuned from the resonant excitation conditions. Both pictures are complementary and helpful in a full understanding of the main features of the numerical results presented in this and the other cited work. We shall see, however, that intuitively attractive explanations of all these features can be given entirely in terms of the time-dependent picture. For the actual numerical applications our time-dependent formulation is not only easier but it seems to be the only practically feasible one when the theory is applied to analyze details of the Auger spectra for systems with dissociating excited state potentials [18,28,30] $V_d(\boldsymbol{r})$ and/or coordinate-dependent decay matrix elements $W_f(\boldsymbol{r})$.

C. Applications to diatomic molecules

For a diatomic molecule, the set of nuclear coordinates $\boldsymbol{r}$ is a set of three components of a vector connecting both nuclei, and all potentials are spherically symmetric: $V_\alpha(\boldsymbol{r}) = V_\alpha(r)$ where $r=|\boldsymbol{r}|$. Therefore, all necessary wave functions, $\psi_{\rm in}(\boldsymbol{r})$, $\phi_d(\boldsymbol{r},t)$, and $\varphi^f_\chi(\boldsymbol{r})$, can be expanded into series involving spherical harmonics $Y_{lm}(\hat{\boldsymbol{r}})$ ($\hat{\boldsymbol{r}}$ is a unit vector along $\boldsymbol{r}$). For the duration of the scattering process much shorter than the molecular rotation period the scattering cross section may be evaluated in a sudden approximation with frozen molecular orientation and, in view of the forthcoming averaging over molecular orientation [38], the initial wave packet may be taken spherically symmetric (corresponding to the rotational ground state of the molecule). It remains spherically symmetric throughout its time evolution; so when the scalar product is taken with $\varphi^f_\chi(\boldsymbol{r})$ in Eq. (22), only the s-wave component of the latter contributes. This allows us to rewrite the expression for the cross section in a form in which only one-dimensional integrals occur. We also see that these symmetry arguments must be modified if the $\boldsymbol{r}$ dependence of the molecular dipole moment transition matrix element $\boldsymbol{D}(\boldsymbol{r})$ is not ignored.

The summation over χ in Eq. (22) runs over both localized and extended energy eigenstates of H_f. From now on we consider only one Auger decay mode and introduce the energy scale with the origin at the asymptotic value of $V_f(r)$, i.e.,

$$\lim_{r\to\infty} V_f(r) = 0, \tag{28}$$

so the energy corresponding to the localized states in this potential is negative and that for the extended states is positive. For the latter, the wave functions $\varphi^f_\chi(\boldsymbol{r})$ must satisfy the incoming boundary condition for its scattered wave component and the summation over χ must eventually be converted into an integration. Details are given in Appendix B and here we list the results only.

The cross section in Eq. (22) consists of two contributions,

$$\frac{d^2\sigma_e(\mathcal{E})}{d\mathcal{E}d\Omega} = \left(\frac{d^2\sigma_e(\mathcal{E})}{d\mathcal{E}d\Omega}\right)^{\rm loc} + \left(\frac{d^2\sigma_e(\mathcal{E})}{d\mathcal{E}d\Omega}\right)^{\rm ext}, \tag{29}$$

in which the summation over χ runs over the localized and the extended eigenstates of H_f, respectively. Following the procedure described in Appendix B we get

$$\left(\frac{d^2\sigma_e(\mathcal{E})}{d\mathcal{E}d\Omega}\right)^{\rm loc} = \left[\frac{1}{4\pi\epsilon_0}\right]\frac{\Gamma_f\omega_L D^2}{2c\hbar^3}\sum_{n'} G((E^f_{n'}+\mathcal{E}-E_{\rm in}-\hbar\omega_L)/\hbar) \times \left|\int_0^\infty dt e^{(i/\hbar)(E^f_{n'}+\mathcal{E})t}\, e^{-\Gamma t/2\hbar}\langle u^f_{n'}|u_d(t)\rangle\right|^2, \tag{30a}$$

$$\left(\frac{d^2\sigma_e(\mathcal{E})}{d\mathcal{E}d\Omega}\right)^{\rm ext} = \left[\frac{1}{4\pi\epsilon_0}\right]\frac{\Gamma_f\omega_L D^2}{2c\hbar^3}\int_0^\infty dq G((E(q)+\mathcal{E}-E_{\rm in}-\hbar\omega_L)/\hbar) \times \left|\int_0^\infty dt e^{(i/\hbar)(E(q)+\mathcal{E})t}\, e^{-\Gamma t/2\hbar}\langle u^f(q)|u_d(t)\rangle\right|^2. \tag{30b}$$

Here, $\langle\ |\ \rangle$ is a one-dimensional integration over r involving the radial wave functions defined below. Thus $u_d(r,t)$ is a solution of the time-dependent one-dimensional Schrödinger equation involving the core-excited state potential energy $V_d(r)$ (μ is the effective mass of the relative motion of both constituents of the molecule):

$$\left(-\frac{\hbar^2}{2\mu}\frac{\partial^2}{\partial r^2}+V_d(r)\right)u_d(r,t) = i\hbar\frac{\partial}{\partial t}u_d(r,t), \tag{31}$$

with the initial condition $u_d(r,t=0)=u_{\rm in}(r)$ which is the one-dimensional ground state wave function in the ground state potential $V_g(r)$:

$$\left(-\frac{\hbar^2}{2\mu}\frac{d^2}{dr^2}+V_g(r)\right)u_{\rm in}(r) = E_{\rm in}u_{\rm in}(r). \tag{32}$$

Next, $u^f_{n'}(r)$ in Eq. (30a) is the bound state wave function, corresponding to the energy eigenvalue $E^f_{n'}<0$, of the one-dimensional Schrödinger equation involving $V_f(r)$:

$$\left(-\frac{\hbar^2}{2\mu}\frac{d^2}{dr^2}+V_f(r)\right)u^f_{n'}(r) = E^f_{n'}u^f_{n'}(r). \tag{33}$$

Here and in what follows we use a prime to label the vibrational levels in $V_f(r)$, i.e., $n'=0',1',2',\ldots$. Finally, $u^f(r,q)$ in Eq. (30b) is the extended state wave function of the same Schrödinger equation corresponding to the energy eigenvalue $E(q)=\hbar^2q^2/2\mu$ [with the asymptotic condition (28) there is no need for the superscript f in $E(q)$]. Its normalization is fixed by requiring that for $r\to\infty$ we have

$$u^f(r,q)\to\sqrt{\frac{2}{\pi}}\sin[qr+\delta^f_0(q)], \tag{34}$$

where $\delta_0^f(q)$ is the s-wave phase shift (its value will not be needed).

D. Qualitative properties of the electron spectra

Before going into specific numerical examples it is worthwhile to discuss qualitative features of the expressions in Eqs. (30) for the electron spectra. In particular, we would like to show how the early and the late stages of the time evolution of the wave packet can be accessed by varying the frequency of the nearly monochromatic x-ray radiation and how the electron spectra are affected by the time span over which the spectra are formed.

We reiterate that we deal here with a coherent process in which the photon absorption and the subsequent electron emission cannot be considered as two independent steps. Therefore the energy does not have to be conserved in each step separately but only in the entire process. If the photon $\hbar\omega$ is absorbed and the ion is left in the vibrational state n' after an electron with the kinetic energy $\mathcal{E}$ is emitted, then $E_{\rm in}+\hbar\omega=E_{n'}^f+\mathcal{E}$. Consequently, for nearly monochromatic radiation of the nominal frequency ω_L [i.e., fairly narrow $G(\omega-\omega_L)$ in Eq. (30a)], peaks are expected in the electron spectra for electron energies equal to

$$\mathcal{E}_{n'}^{\rm peak}(\omega_L)=\hbar\omega_L+E_{\rm in}-E_{n'}^f. \tag{35}$$

The time evolution of the wave packet is exponentially damped so the main contribution to the time integral in Eq. (30a) comes from the time span corresponding to the core-excited state lifetime $2\hbar/\Gamma$. In other words, the time-dependent wave packet [or, rather, its overlap with $u_{n'}^f(r)$] contributes effectively to the formation of the spectra for a time no longer than it is permitted by the lifetime. This relevant time evolution may be, as discussed below Eq. (23), further shortened and the result rendered smaller by the destructive oscillations of the t-dependent integrand. The time-dependent wave packet contains components oscillating with frequencies $E_v^d/\hbar$ corresponding to the vibrational energy levels of the core-excited molecule [cf. Eq. (25)]. Therefore, as seen from Eqs. (24) and (30a), only for electron energies $\mathcal{E}$ satisfying the condition

$$|\mathcal{E}+E_{n'}^f-E_v^d|\ll\frac{\Gamma}{2} \tag{36}$$

are the destructive oscillations not present for one particular (vth) component of the wave packet. This component effectively contributes to the formation of the electron spectrum at the energy $\mathcal{E}$ for as long as it is permitted by the actual core hole lifetime $2\hbar/\Gamma$, and its contribution at this energy dominates over the contributions due to all other components of the wave packet. For electron energies $\mathcal{E}$ for which no (n',v) pair can be found for which the condition (36) is satisfied the most significantly contributing components of the wave packet contribute, according to Eqs. (23) and (24), for times shorter than the core hole lifetime and the resulting value of the cross section is relatively small.

The conditions most favorable for relatively large cross sections are met when the nominal radiation frequency is chosen in such a way that possible electron energy peak positions, given in Eq. (35), coincide with the energies $\mathcal{E}$ for which the condition (36) can also be satisfied. This is achieved by tuning the radiation resonantly to the energy difference between the vth vibrational level of the core-excited molecule and the initial ground state of the system

$$\hbar\omega_L=E_v^d-E_{\rm in}\equiv\hbar\omega_L^v \tag{37}$$

for some fixed v. Under such *resonant tuning conditions* (to be referred to as ''resonant primary excitation conditions'') the peak positions in the electron spectra, given in Eq. (35), occur at the energies

$$\mathcal{E}_{n'}^{\rm peak}(\omega_L^v)=E_v^d-E_{n'}^f, \tag{38}$$

which may formally be labeled by both v and n'. For resonantly tuned radiation the time-dependent wave packet contributes to the formation of the spectra around the peaks for the longest possible times limited only by the actual lifetime of the core hole. Consequently, according to Eq. (38), each peak in the electron spectrum may be viewed to be a result of the *energy conserving* Auger transition from the vibrational intermediate state v of the core-excited molecule to the vibrational final level n' of the resulting molecular ion. These peaks will be labeled with $v\searrow n'$ in the graphs which correspond to the resonant primary excitation of the molecule to the vibrational level v (e.g., $0\searrow 0'$, $1\searrow 0'$, $0\searrow 1'$, etc.).

Our main interest in this work is to contrast the time-dependent formation of the spectra for resonant tuning conditions described above with the formation of the spectra when the resonant tuning conditions are not met. When the radiation detuning energy $\hbar\Omega\equiv|E_{\rm in}+\hbar\omega_L-E_v^d|=\hbar|\omega_L-\omega_L^v|$ is, for any v, much larger than $\Gamma/2$ then, according to Eq. (24), the time-dependent wave packet contributes to the formation of the spectra for times shorter than the actual lifetime $2\hbar/\Gamma$ of the core-excited state and this, as we shall see, may dramatically affect the appearance of the electron spectra.

III. NUMERICAL RESULTS

We are going to present a number of calculated electron spectra for two model systems, diatomic N_2 and CO molecules, to illustrate how their features vary with varying energy of the exciting radiation, and how they depend on the types of potential curves involved. To demonstrate the influence of photon bandwidth, we use two values for N_2, one above and one below the core hole lifetime width. To emphasize some different aspects of the spectra we will also devote a shorter subsection to CO using the photon bandwidth from recent experiments [9]. Infinite resolution of the electron energy analyzer is assumed, but some remarks as to its influence will be made.

A. Model potentials and system parameters

We specify now all the potentials to determine the wave functions to be used in the numerical work. The most convenient analytical form for *bonding* potentials is the Morse potential form. For the final ionic state potential we write it as

$$V_f(r)=V_f(e^{-2\gamma_f(r-r_f)}-2e^{-\gamma_f(r-r_f)}). \tag{39}$$

It satisfies the asymptotic condition (28). For the electronic ground and the core-excited state potentials, respectively, we choose, apart from an additive constant,

$$V_g(r)=V_g(e^{-\gamma_g(r-r_g)}-1)^2, \tag{40}$$

$$V_d(r)=V_d(e^{-\gamma_d(r-r_d)}-1)^2. \tag{41}$$

Besides the equilibrium position, r_α ($\alpha=g,d$ or f), each of the potentials has also two other parameters, the potential depth V_α and the range parameter γ_α, which are chosen to fit the experimental spectroscopic data, i.e., the frequency at the bottom of the potential, ω_α, and the anharmonicity, $\omega_\alpha x_\alpha$, of the potential:

$$V_\alpha=\frac{(\hbar\omega_\alpha)^2}{4\hbar\omega_\alpha x_\alpha}, \tag{42}$$

$$\gamma_\alpha=\sqrt{2\mu\hbar\omega_\alpha x_\alpha}/\hbar. \tag{43}$$

This usually results in Morse potentials with a dissociation energy $D_\alpha=\hbar\omega_\alpha(1-x_\alpha)^2/4x_\alpha$ (i.e., the energy difference between the asymptotic value of potential and the energy of its ground state) which underestimates its actual value. This could be a problem for particularly weakly bonding final ionic potentials $V_f(r)$ (as in one of the numerical examples presented in this work), and in such cases a reasonable compromise must be made in choosing the Morse potential parameters. A dimensionless parameter

$$\sigma_\alpha=\sqrt{2\mu V_\alpha}/\hbar\gamma_\alpha=1/2x_\alpha \tag{44}$$

is often used to characterize Morse potentials. The number of bound states in the Morse potential $V_\alpha(r)$ is equal to the largest integer smaller than $\sigma_\alpha-1/2$.

The expressions in Eqs. (40) and (41) account only for the functional shape of the two potentials, and appropriate constant energies should be added to each of them to account for their placement on the energy scale with respect to the origin defined in Eq. (28). We do not do this explicitly here because the constant energy which must be added to $V_g(r)$ does not affect the shape of the initial wave packet $u_d(r)$, and the constant to be added to $V_d(r)$ results only in a time-dependent phase factor in the time-dependent wave packet $u_d(r,t)$ which can be taken care of separately. Furthermore, if the cross section is expressed in terms of the relative nominal radiation frequency and the relative Auger electron energy defined, respectively, as

$$\omega_L^{\rm rel}=\omega_L-(E_0^d-E_{\rm in})/\hbar, \tag{45a}$$

$$\mathcal{E}^{\rm rel}=\mathcal{E}-(E_0^d-E_{0'}^f), \tag{45b}$$

then it no longer depends explicitly on these additive constant energies. Here, E_0^d is the energy of the vibrational ground state in the core-excited state potential $V_d(r)$ and $E_{0'}^f$ is the energy of the ground ($n'=0'$) state in the final ionic configuration potential $V_f(r)$ [both energies are measured with respect to the energy zero defined in Eq. (28)]. In other words, $\omega_L^{\rm rel}=0$ corresponds to the radiation resonantly tuned to the energy difference between the initial state (ground state of the electronic ground state of the molecule) and the vibrational $v=0$ ground state of the core-excited molecule. Similarly, $\mathcal{E}^{\rm rel}=0$ corresponds to the kinetic energy of an electron emitted by the decaying core-excited molecule in its vibrational $v=0$ ground state which leaves the molecular ion in its vibrational $n'=0'$ ground state. All numerical results in this paper are presented in terms of these relative radiation frequencies and relative Auger electron energies.

The Morse potentials allow us to obtain analytic expressions for the wave functions used in both expressions, Eqs. (30), for the cross section. They are not needed for the discussion to follow so we list them in Appendix C: in Eqs. (C1), (C3), and (C4) the expressions for the initial wave packet $u_{\rm in}(r)$, for the bound state wave functions $u_{n'}^f(r)$, and for the corresponding energy eigenvalues $E_{n'}^f$, respectively, are given. The time evolution of the wave packet is followed numerically, although approximating the initial wave packet by a Gaussian given in Eq. (C2) and using Heller's [34] semiclassical method of solving the time-dependent Schrödinger equation it is possible to derive an approximate algebraic expression also for the time-dependent wave packet $u_d(r,t)$. The exact numerical solution is used, however, in this work. For the extended state wave function $u^f(r,q)$ the most convenient expression is provided using the WKB approximation. For the Morse potential $V_f(r)$ such an expression has a simple analytic form which is listed in Eqs. (C5)–(C7).

Cross sections given in Eqs. (30) have a dimension of *length*^{2}/*energy* so it is convenient to introduce the dimensionless electron spectrum, $S(\mathcal{E}^{\rm rel})$, by dividing the cross section in Eq. (29) with

$$\left[\frac{1}{4\pi\epsilon_0}\right]\frac{\Gamma_f\omega_L D^2}{2c\hbar^3\omega_d^3}, \tag{46}$$

where ω_d is the vibrational frequency at the bottom of the core-excited state potential $V_d(r)$. Implicitly, the energy spectrum depends also on the relative radiation frequency $\omega_L^{\rm rel}$. Note that Γ_f, which determines the branching ratio between different Auger decay modes, is included in the dimensional factor of Eq. (46). So, while it makes sense to compare the magnitudes of different calculated spectra for the same final electronic configuration, one should not pay too much attention to the relative magnitudes of the spectra for different final states.

The parameters used in the calculations are listed in Table I for both systems. The effective masses for N_2 and CO are [39] $\mu=1.1628\times10^{-26}$ kg, and $\mu=1.1392\times10^{-26}$ kg, respectively. Apart from the spectroscopic parameters, frequency ω_α, anharmonicity $\omega_\alpha x_\alpha$, and bond length r_α, for each of the potentials $V_\alpha(r)$ involved, the lifetime parameter for the core-excited state is also needed. The values $\Gamma=132$ meV [40] for N_2 and $\Gamma=97$ meV [9] for CO are accepted. Some additional comments on the choice of the parameters are made in the following subsections in which the results are presented and discussed.

Before continuing, a note concerning the numerical strategy adopted to compute the Auger electron spectra is in order. First, the time-dependent wave packet $u_d(r,t)$ is propa-

TABLE I. Parameters of the potentials in Eqs. (39)–(41) for N_2, N_2^+, CO, and CO^+.

	$\hbar\omega_\alpha$ (meV)	$\hbar\omega_\alpha x_\alpha$ (meV)	r_α (Å)
$N_2(X\ ^1\Sigma_g^+)$[a]	292.426	1.7760	1.09768
$N_2[1s^{-1},1\pi_g]$[b]	235.2	1.9	1.164
$N_2^+[3\sigma_g^{-1}]$ $(X\ ^2\Sigma_g^+)$[c]	273.633	1.996	1.1163
$N_2^+[1\pi_u^{-1}]$ $(A\ ^2\Pi_u)$[c]	236.029	1.862	1.1747
$N_2^+[1\pi_u^{-2},1\pi_g]$ $(D\ ^2\Pi_g)$[d]	116.16	1.406	1.471
CO $(X\ ^1\Sigma^+)$[e]	269.023	1.648	1.1283
CO $[C\ 1s(2\sigma)^{-1},2\pi]$[f]	258.327	1.899	1.1529
$CO^+[5\sigma^{-1}](X\ ^2\Sigma^+)$[g]	274.531	1.880	1.1151
$CO^+[1\pi^{-1}](A\ ^2\Pi)$[g]	193.671	1.678	1.2437
$CO^+[4\sigma^{-1}](B\ ^2\Sigma^+)$[g]	215.011	3.463	1.1687

[a] $\alpha=g$; Ref. [39].
[b] $\alpha=d$; Ref. [40].
[c] $\alpha=f$; Ref. [15].
[d] $\alpha=f$; Ref. [42], modified in Ref. [29].
[e] $\alpha=g$; Refs. [15,9].
[f] $\alpha=d$; Refs. [15,9].
[g] $\alpha=f$; Refs. [15,9].

gated by solving numerically the Schrödinger equation (31) and the result is stored in a file to be used in the subsequent computations. The wave-packet evolution needs to be computed only once for a given molecule because it depends only on the shapes of the $V_g(r)$ and $V_d(r)$ potentials. We have found that it suffices to propagate the wave packet for no more than five oscillation periods $2\pi/\omega_d$ and store the result at 100 time increments per each oscillation period on a grid of 64 equally spaced points between $r=0.96$ Å and 1.46 Å for N_2, and between $r=0.92$ Å and 1.41 Å for CO (cf. system parameters in Table I). The wave packet is negligibly small outside these ranges for all times. Next, all needed overlaps under the time integrals in Eqs. (30) are computed and stored for all time instants for all bound states n' in Eq. (30a) and for sufficiently densely sampled energies $E(q)$ in Eq. (30b) (the latter has to be done only for the spectator decay for N_2 and the sampling density should be roughly correlated with the smallest radiation bandwidth to be used). The remaining integrations over time [and over $E(q)$ in Eq. (30b) if needed] are done using cubic splines. Only at the latter stage must the lifetime parameter Γ, the radiation central frequency, the radiation bandwidth, and the actual electron energies be specified.

B. Results for the nitrogen molecule (N_2)

Three different final electronic configurations of the N_2^+ ion are considered. Two of them result from the participant decay of the core-excited state to the $[3\sigma_g^{-1}]$ and to the $[1\pi_u^{-1}]$ ionic configurations for which the parameters of the ground state $N_2^+(X\ ^2\Sigma_g^+)$ and of the excited state $N_2^+(A\ ^2\Pi_u)$ are used [15], respectively. The third final configuration is $[1\pi_u^{-2},1\pi_g]$ and results from a spectator decay of the core-excited state. It has been shown [41] to be the dominant decay channel which may eventually lead to $N_2^+ \rightarrow N(^4S^o)+N^+(^3P)$ fragmentation. We adopt for it parameters which are slightly modified from the spectroscopic parameters of $N_2^+(D\ ^2\Pi_g)$ (i.e., from $\hbar\omega_f=112.69$ meV and $\hbar\omega_f x_f=1.509$ meV) which would result directly from the experimentally established classical turning points for the 11 lowest bound states of Namioka *et al.* [42]. The modification [29] aims at removing a significant underestimate of the depth of $V_f(r)$ (which should be equal to 2.4 eV) and is necessary in view of the fact that the Auger electron spectrum is expected to extend over some 5 eV and is formed by electrons which leave the molecular N_2^+ ion with enough energy to either dissociate into N and N^+ or to leave it merely vibrationally excited.

We note also that the parameters of the ground state potential determine solely the shape of the initial wave packet. Although the effect of the anharmonicity on its shape is almost invisible to the eye, the following time evolution seems to be quite sensitive to this minute difference. For example, in the N $1s\rightarrow 1\pi_g$ absorption spectrum calculated using the time-dependent approach without the anharmonicity of the ground state the $v=0$ peak is about 9% lower than the $v=1$ peak but the difference is reduced down to about 2% when the correct anharmonicity is included [29]. Experimentally both peaks are of approximately equal height [40] so in all calculations presented here we do account for the anharmonicity of the ground state.

We further note certain similarities and differences among different potentials listed in Table I. The potentials for the neutral and ionic ground states are very similar: their frequency parameters and equilibrium bond lengths differ by less than 7%, and 2%, respectively. Even closer to each other are the potentials of the $N_2[1s^{-1},1\pi_g]$ core-excited state and the $N_2^+(A\ ^2\Pi_u)$ state of the ion: the corresponding differences are less than 0.3% and 1%, respectively. These figures should be compared with the differences of roughly 20% and 6%, respectively, between the parameters of these two groups of pairs. The ionic potential resulting from the spectator decay stands apart because of its relatively large bond length, small frequency parameter, and low dissociation energy. Consequently, in comparison with the participant final states, the vibrational energy levels in the spectator final state potential are quite densely distributed and the overlap between the extended states of this potential and the eigenfunctions of the core-excited state Hamiltonian H_d is significant.

As already mentioned when relative energies in Eqs. (45) were introduced, the functional shapes of the Auger electron spectra do not depend explicitly on the actual radiation frequency and the actual electron energy, but rather on their ''relative'' values defined there. Thus it is convenient to use these relative variables as independent variables in all figures to follow. Then, the actual nominal radiation frequency can be found by adding, according to Eq. (45a), the energy [40] $T_{00}\equiv E_0^d-E_{\rm in}=400.868$ eV to $\hbar\omega_L^{\rm rel}$. The energy which must be added according to Eq. (45b) to the relative electron energy in order to get the actual kinetic energy of the Auger electrons depends on the actual mode of the Auger decay. Therefore the corresponding values are given in the figure captions.

All calculated spectra are presented in Figs. 1–6. The panel on the right-hand side of each figure shows the relevant potential curves using solid lines: $V_g(r)$ (the lowest curve), $V_d(r)$ (the highest curve), and the ''active'' $V_f(r)$ (the intermediate curve) used to calculate the spectra. The

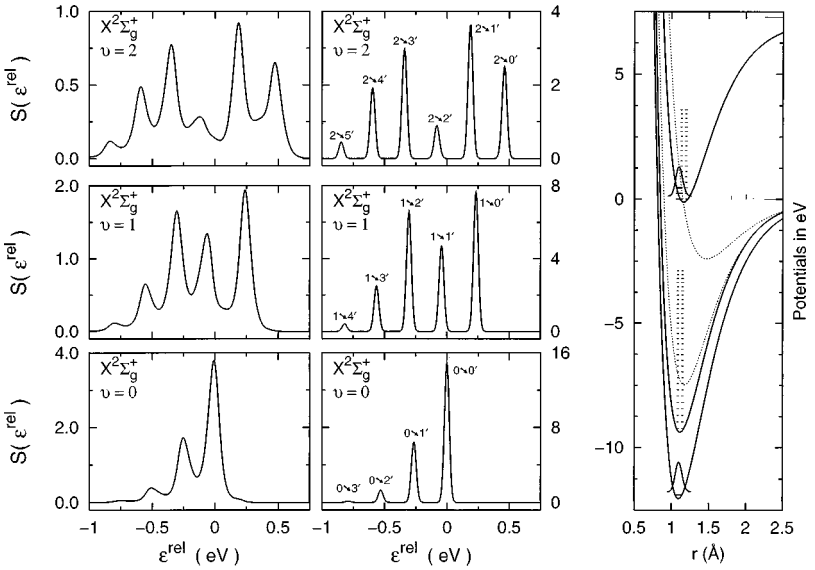

FIG. 1. Auger electron energy spectra for participant decay of the N_2 $1s$-hole excited (core-excited) state to the $[3\sigma_g^{-1}](X\ ^2\Sigma_g^+)$ state of the N_2^+ ion for monochromator resolutions with FWHM $\Gamma_L=200$ meV (left panels) and $\Gamma_L=50$ meV (right panels) and the core-excited state lifetime width $\Gamma=132$ meV. $v=0,1$, and 2 denote the quantum numbers of the vibrational levels of the core-excited state to which the nominal radiation frequency is resonantly tuned. In the right panels the peaks are labeled by identifying the resonant transitions from the level $v=0$, 1, or 2 to the final vibrational level $n'=0',1',\ldots$ of the N_2^+ ion. The actual electron kinetic energy [cf. Eq. (45b)] is $\mathcal{E}=\mathcal{E}^{\rm rel}+T_{00}-15.580$ eV $=\mathcal{E}^{\rm rel}+385.288$ eV [46–48]. See text (fifth paragraph in Sec. III B) for the detailed description of the panel containing the potential energy curves, vibrational energy levels, and the initial wave packet.

remaining two potential curves $V_f(r)$ used to compute the spectra in the other figures are shown for comparison using dotted lines. $V_f(r)$ curves are placed along the energy axis according to the convention chosen in Eq. (28) and the same asymptotic value of 0.0 eV is chosen for $V_g(r)$. $V_d(r)$ is placed in such a way that its ground vibrational level $v=0$ is at $E=0.0$ eV. Several vibrational v and n' levels are shown above the minimum of $V_d(r)$ and of the active $V_f(r)$, respectively. The initial wave packet is shown at $V_g(r)$ along with the horizontal bar representing its eigenenergy $E_{\rm in}$. The wave packet is repeated at its initial position with respect to the $V_d(r)$ potential curve. Three thicker horizontal lines placed under the upper replica of the initial wave packet indicate three relative energies $\hbar\omega_L^{\rm rel}$ with respect to the potential $V_d(r)$ (and its energy levels), to which the x-ray radiation is nominally tuned in the spectra shown in the horizontal panels of the particular figure. Finally, the height of three vertical bars (at 0 eV) represent, counting from the leftmost one, the lifetime parameter Γ, and two x-ray bandwidths Γ_L used in the calculations.

The Auger electron spectra for the participant $N_2[1s^{-1},1\pi_g]\rightarrow N_2^+[3\sigma_g^{-1}](X\ ^2\Sigma_g^+)$ Auger decay, normalized according to Eq. (46) and calculated using Eq. (30a), are shown in Figs. 1 and 2 for two radiation FWHM's, $\Gamma_L=200$ and 50 meV (left and right hand panels, respectively). In Fig. 1, three nominal radiation frequencies $\hbar\omega_L^{\rm rel}=0$, $\hbar\omega_L^{\rm rel}=E^d_{v=1}-E^d_0=231.39$ meV, and $\hbar\omega_L^{\rm rel}=E^d_{v=2}-E^d_0=459.11$ meV corresponding, respectively, to the *resonant* excitations to $v=0,1$, and 2 vibrational levels of the core-excited state are used (panels denoted $v=0,1$, and 2, respectively). The spectra resulting from *off-resonant* excitations are shown in the two lower panels in Fig. 2 (in the top panels the resonant $v=0$ excitation case is shown again for comparison on an expanded energy scale). The notation $v=-2/3$ means that the nominal radiation frequency is lower than that needed for the resonant $v=0$ excitation by two-thirds of the $v=0$ to $v=1$ separation, i.e., $\hbar\omega_L^{\rm rel}=-154.26$ meV for $v=-2/3$, and twice that for $v=-4/3$. Equation (C4), with γ_d and σ_d substituted for γ_f and σ_f, respectively, was used to get the $E^d_v-E^d_0$ values quoted above. The contribution due to Eq. (30b) is negligible because this mode of the Auger decay does not lead to fragmentation of the ion.

The Auger electron spectra for another participant decay, $N_2[1s^{-1},1\pi_g]\rightarrow N_2^+[1\pi_u^{-1}](A\ ^2\Pi_u)$, are shown in Figs. 3

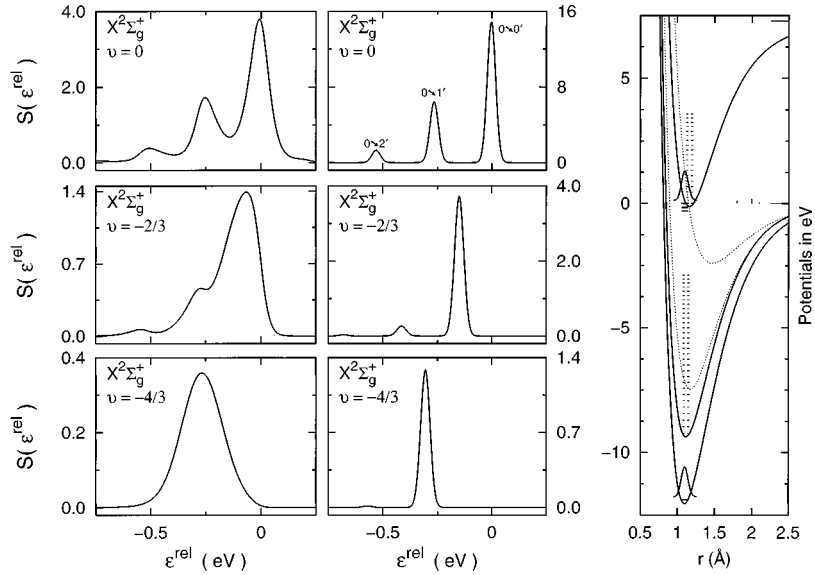

FIG. 2. The same as in Fig. 1 but for the nominal radiation frequency tuned to (top panel) and below the $v=0$ resonant excitation by two-thirds (middle panels) and four-thirds (bottom panels) of the energy difference between the two lowest vibrational levels of the core-excited state.

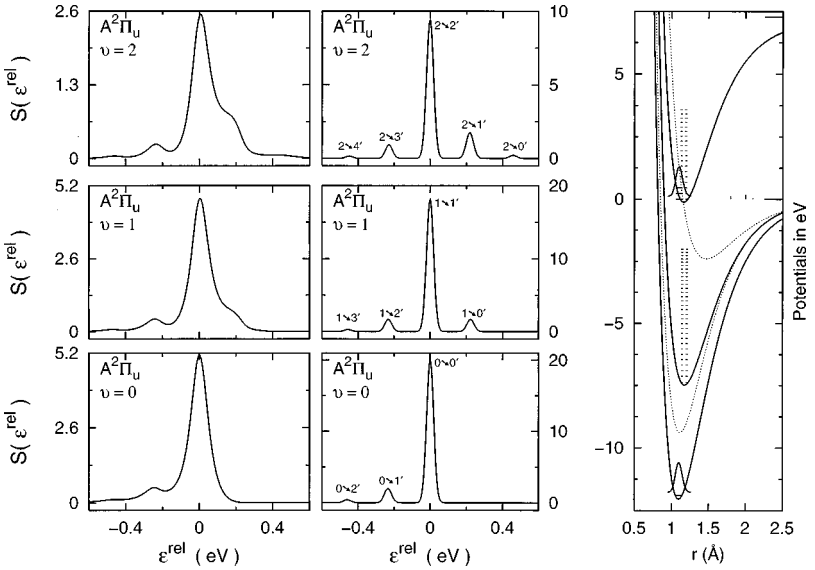

FIG. 3. The same as in Fig. 1 but for the spectator decay to $[1\pi_u^{-1}](A\ ^2\Pi_u)$ state of the N_2^+ ion. Actual electron kinetic energy: $\mathcal{E}=\mathcal{E}^{\rm rel}+T_{00}-16.92$ eV$=\mathcal{E}^{\rm rel}+383.948$ eV [46–48].

and 4 for resonant and nonresonant excitations, respectively, using the same radiation frequencies and linewidths as in the corresponding panels of Figs. 1 and 2. Again, the contribution due to Eq. (30b) is negligible in Figs. 3 and 4.

The Auger electron spectra for the spectator decay, $N_2[1s^{-1},1\pi_g]\rightarrow N_2^+[1\pi_u^{-2},1\pi_g](D\ ^2\Pi_g)$, are shown in Figs. 5 and 6 in the same general setup as for the other spectra. In this case, however, owing to the significantly larger equilibrium bond length of the molecular ion and its significantly smaller dissociation energy as compared to the other two cases, the contribution due to Eq. (30b) is significant. The vertical arrows indicate the electron energies below which the molecular ion left behind dissociates into $N(^4S^o)$ and $N^+(^3P)$. Both contributions in Eq. (29) overlap around the energy indicated by the vertical arrow over the interval roughly equal to Γ_L. We note here that the photodissociation cross section and the time of flight spectra of the dissociation fragments resulting from this particular spectator decay were calculated before using essentially the same approach [29] [cf. Eq. (17a) and the text below it].

For the discussion of the main features of the spectra presented in Figs. 1–6 we can use the framework of either the time-dependent or the time-independent version of the theory; the latter gives a better conceptual insight into the processes. Therefore we will use Eq. (30a) to gain a qualitative understanding of the observed features. Similar discussion can be made for the contribution given in Eq. (30b).

The $(v\searrow n')$ peaks [cf. Eq. (38) and the text below for the meaning of this notation] for the resonant tuning conditions have been identified only in the high-resolution panels of Figs. 1 and 3 in which the radiation was resonantly tuned according to Eq. (37) to $\omega_L^{v=0}$, $\omega_L^{v=1}$, and $\omega_L^{v=2}$ in panels labeled $v=0$,1, and 2, respectively. In Fig. 5 the number of such peaks is 41 [the number of bound states in $V_f(r)$], too large to be individually labeled in the graphs. The peak $(0\searrow 0')$ which should appear at $\mathcal{E}^{\rm rel}=0$ in the lowest right hand panel in Fig. 5 is invisible on the scale of the graph and the fringe of $(v\searrow n')$ peaks for $n'\gtrsim 5$ is seen for energies $\mathcal{E}^{\rm rel}\lesssim -0.54$ eV. The $(0\searrow 40')$ peak would appear just to the right of the vertical arrow in this panel if it could be resolved. Recall that the spectra for energies lower than those indicated by the vertical arrow in all panels in Fig. 5 are due to the Auger decay transitions which eventually lead to the dissociation of the molecular ion.

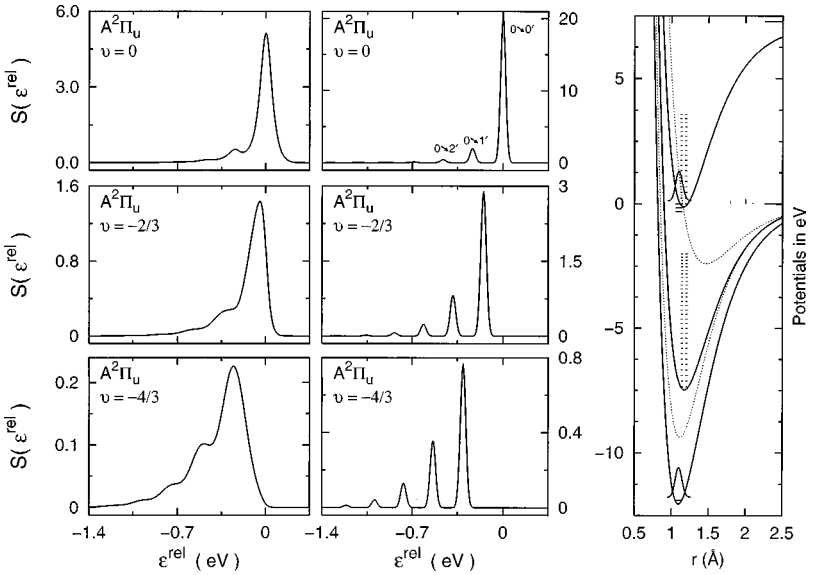

FIG. 4. The same as in Fig. 2 but for the spectator decay to $[1\pi_u^{-1}](A\ ^2\Pi_u)$ state of the N_2^+ ion.

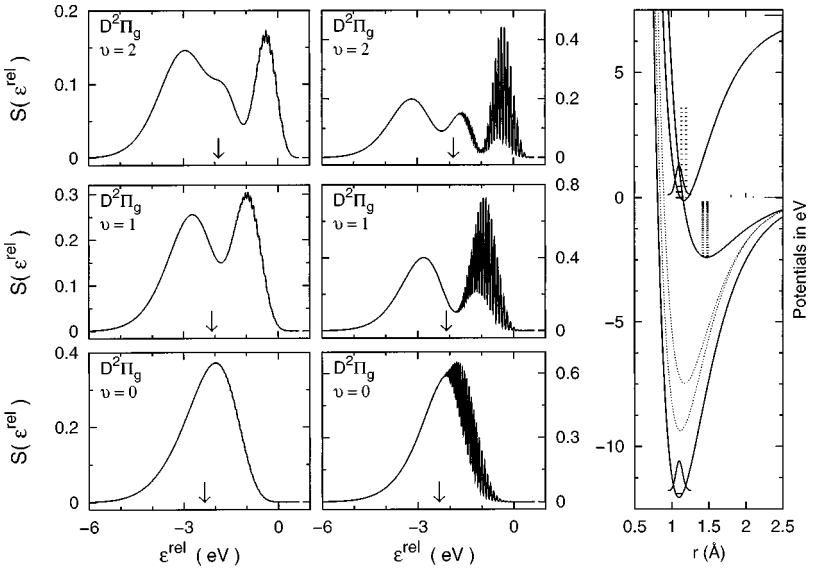

FIG. 5. The same as in Fig. 1 but for the participant decay to $[1\pi_u^{-2},1\pi_g](D\ ^2\Pi_g)$ state of the N_2^+ ion. The individual peaks (41 of them) are not labeled in the right panels. The vertical arrow indicates the energy below which the contribution (30a) to the total cross section due to the nondissociating final states of the ion sharply drops down and the contribution (30b) due to the dissociating final states sharply takes over. Actual electron kinetic energy: $\mathcal{E}=\mathcal{E}^{\rm rel}+T_{00}-22.03$ eV$=\mathcal{E}^{\rm rel}+378.838$ eV [42,47].

As expected from energy conservation all peaks in Figs. 1, 3, and 5 move up in energy by 231.39 meV with respect to their positions in the $v=0$ panel when ω_L is tuned to $\omega_L^{v=1}$ or by 459.11 meV when it is tuned to $\omega_L^{v=2}$.

For the radiation resonantly tuned to ω_L^v, only the vth component of the time-dependent wave packet contributes to the spectrum for the entire lifetime $2\hbar/\Gamma$ of the core-excited state. Therefore the overlap of that particular vth component with the wave function of the final vibrational level n' decides how high the peak $(v\searrow n')$ is. All other vibrational v components of the time-dependent wave packet contribute to the formation of the spectra for such short times—due to their rapid oscillations in time [cf. Eqs. (23) and (24) and the discussion around them]—that they are effectively wiped out in comparison with the resonantly excited component.

For the spectator decay, the evolution of the spectra in Fig. 5, as the tuning condition (36) is met consecutively for different v's, may be roughly understood using arguments based on the reflection approximation because (i) the extended states of the final state of the ion contribute significantly to the spectra (the parts of the spectra to the left of the vertical arrows), and (ii) the vibrational levels of the final state, which contribute to the spectra to the right of the vertical arrows, are closely spaced in energy and correspond to rather high quantum numbers n' (making them somewhat similar to the extended state wave functions). Consequently, the electron spectra in the right hand panels of Fig. 5 reflect the nodal structure of the vibrational wave functions of the core-excited molecule: (i) the $v=0$ ground vibrational state wave function of the core-excited state does not have any nodes, so the $v=0$ electron spectrum in Fig. 5 has one broad maximum enveloping the individual peaks; (ii) the wave functions of the $v=1$ and $v=2$ vibrational levels which, respectively, contribute to the formation of the spectra for the longest time for the tuning conditions in the $v=1$ and $v=2$ panels have one and two nodes, respectively, so one and two deep minima are seen in the corresponding panels in Fig. 5. The spectra do not go all the way down to zero at the minima (as expected from the above node-based argument) because other vibrational v components do contribute something even though their ''effective'' lifetime is short, and because the reflection approximation arguments do not apply

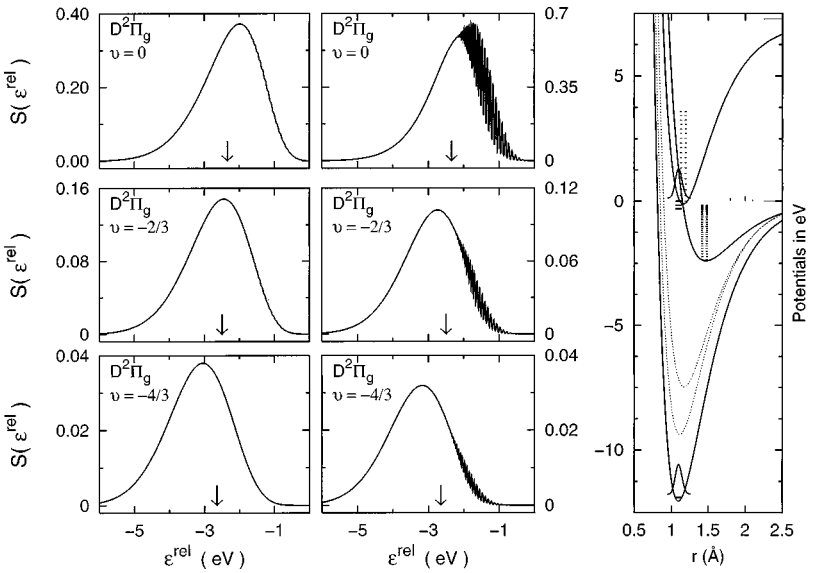

FIG. 6. The same as in Fig. 2 but for the participant decay to $[1\pi_u^{-2},1\pi_g](D\ ^2\Pi_g)$ state of the N_2^+ ion. The remaining comments are as in Fig. 5.

rigorously. The spectra in the left hand panels of Fig. 5 look then as one would expect them to do when high-resolution structure is smoothed out by poorer radiation resolution. We note in passing that the presence of this node-related structure in the time of flight spectra of the dissociation products of the resonantly core-excited N_2 molecule after it decays in this particular spectator Auger decay mode was already theoretically derived and discussed in Ref. [29]. Its presence in the resonant x-ray Raman scattering spectra for dissociating final states was derived and discussed in detail in Ref. [28] and was recently observed and interpreted [13] in ARRE spectator spectra for core-excited CO.

The reflection approximation arguments certainly do not apply for the participator decay spectra in Figs. 1 and 3 because here rather low final vibrational levels n' are involved. Actually, one might be surprised to see how little the low-resolution spectra in the left hand panels in Fig. 3 change as the radiation frequency is resonantly tuned to different vibrational states of the core-excited state: the dominant peak does not move and the only change seems to be the appearance of additional weak structures at the high-energy side of the spectra with higher v. A look at the high-resolution counterparts and at the peak identifications there shows that peaks corresponding to given vibrational final states n' move with increasing photon energy as expected from energy conservation but that the ''diagonal'' peak $(v \searrow n')$ (i.e., the one for which $n'=v$) at $\mathcal{E}^{\mathrm{rel}}=0$ dominates each spectrum. This is due to the similarity of the core-excited and the final ionic state potentials, $V_d(r)$ and $V_f(r)$, respectively, for this particular Auger decay (cf. Table I). The vibrational level spacing in both potentials is almost the same; so the $(v \searrow n')$ peaks with $n'=v-\ell$ for a fixed integer ℓ appear at almost the same energy in the spectra corresponding to the radiation tuned to different v's according to Eq. (37). The vth component of the time-dependent wave packet which contributes to the formation of the spectrum for the longest time, and thus contributes dominantly to the spectrum, is almost identical both in shape and in its absolute position to the vibrational wave function with $n'=v$ in the final ionic state. Their overlap is, therefore, much larger than the overlap for any other (v,n') pair causing the diagonal peak $(v \searrow n')$ with $n'=v$ to dominate each spectrum. In fact, if the potential energy curves $V_f(r)$ and $V_d(r)$ were completely identical then the diagonal peak would be the only one present in each spectrum and the spectra in all three panels at a given side (left or right) in Fig. 3 would be completely identical (apart from different overall multiplicative factors).

A very different situation is encountered in the case of the spectra in Fig. 1. There, the potentials $V_d(r)$ and $V_f(r)$ are very dissimilar. Therefore the vth component of the time-dependent wave packet which contributes the longest to the formation of the spectra has significant overlap with an increasingly larger number of different vibrational levels n', as the radiation is tuned to higher v. As a consequence the vibrational structure changes and shifts considerably for different tuning conditions. Another interesting point to note in Fig. 1 concerns the small structure at the high-energy side of the $(0 \searrow 0')$ peak in the left hand $v=0$ panel which is totally absent in the corresponding high-resolution spectrum (the right hand panel). This is, of course, due to the fact that in the case of broad radiation bandwidth a considerable fraction of the radiation energy can resonantly excite the $v=1$ vibration of the core-excited molecule even if the nominal radiation frequency ω_L is tuned to the $v=0$ level.

This brings us to the point where the role played by the finite resolution of the electron detector should be mentioned. Our theoretical spectra are calculated assuming ideal electron detector resolution. The actual experimental resolution is usually represented by a Gaussian resolution profile with which our spectra should be convoluted before being compared with the experimental data. We have not attempted to do this because the effect of such a convolution is a rather trivial broadening of the spectra which does not enrich their structure. Such a convolution *is not equivalent* to the convolution with the x-ray line profile which we do in our theory: i.e., one cannot compensate for a poor x-ray resolution by using the electron detector with higher resolution. For example, in Fig. 1, no convolution of the $v=0$ narrow excitation spectrum (the lowest right hand panel) with an electron detector resolution profile can result in the $v=0$ spectrum for the broad excitation (the lowest left hand panel). In particular, the structure discussed in the preceding paragraph is intimately related to the broad radiation bandwidth and cannot be created by convoluting the narrow bandwidth spectra (where it is absent) with a broad resolution profile of the electron detector. On the other hand, low resolution of the latter will of course wipe out the fine structure in Figs. 5 and 6 (right parts).

The preceding discussion for resonant initial excitation, although deliberately focused on the time-dependent aspect of the problem, could have been based as well on the time-independent picture, using arguments based on Franck-Condon factors and on energy conservation occurring not only for the overall process but approximately also for the excitation and deexcitation steps separately. This is, of course, the result of the fact that all that matters for resonant excitation is a long time evolution of the wave packet during which only one of its vibrational components effectively contributes to the formation of the spectrum for as long as it is permitted by the overall lifetime of the core-excited state. When the radiation is not resonantly tuned to any of the vibrational levels of the core-excited state, then the two-step picture of the process, with energy being conserved in each step separately, is no longer valid. The shape of the spectra then depends on the time-dependent wave packet in a more complicated way. Still, for finite exciting radiation linewidth it is difficult to be completely ''out of tune'' with any of the vibrational levels and one can argue that as the radiation frequency is swept from one resonant frequency given by the condition (37) to the next, the electron spectra continuously evolve from the spectra in the bottom panels of Figs. 1, 3, and 5 through the ones in the middle panels to those at the top. This is indeed the case, and the peaks which for detuned radiation can, as seen from Eq. (35), be labeled by the final vibrational level n' only, shift to the right according to the condition (35) stemming from energy conservation in the overall excitation—deexcitation process. Indeed we have found that, for an intermediate tuning condition of the final state of Fig. 3, detuning with narrow bandwidth to halfway between the $v=0$ and $v=1$ resonances, the spectrum has two peaks of almost equal height rather than only one as in the resonant excitation cases (note that this is not shown in

Fig. 3). This has indeed been reported in the most recent experimental data which just came to our attention [14]: for this same final state a single peak found for $v=0$ and $v=1$ tuning conditions is split into two for detuning halfway between these resonances.

It is more interesting, therefore, to examine truly nonresonant excitation cases for which the detuning energy Ω may be chosen arbitrarily large. The clearest possibility for this is to choose a nominal radiation frequency which is smaller than the smallest energy necessary for resonant excitation, i.e., for $\omega_L < \omega_L^{v=0}$. We note that the same effects occur symmetrically when detuning above the resonance. However, because of the overlap with the excitation of higher vibrations the situation is not as clearcut there. The spectra for $\omega_L < \omega_L^{v=0}$ are shown in the two lower panels of Figs. 2, 4, and 6 (in the top panels the resonant $v=0$ spectra are shown again for comparison).

Here, a new type of behavior is observed. For the $N_2[1s^{-1},1\pi_g] \rightarrow N_2^+[3\sigma_g^{-1}](X\ ^2\Sigma_g^+)$ participant decay in Fig. 2 the spectrum evolves from the one composed of three peaks for the resonant $v=0$ excitation to the spectrum dominated by one peak only for off-resonance tuning conditions. This is an example of the ''collapse of the vibrational structure'' observed [12] and discussed [22] for CO (to which we will return later on). Very recently the collapse demonstrated in Fig. 2 was experimentally observed for this particular case [14]. The reverse is, however, true for the $N_2[1s^{-1},1\pi_g] \rightarrow N_2^+[1\pi_u^{-1}](A\ ^2\Pi_u)$ participant decay in Fig. 4, where the spectrum evolves from the one dominated by essentially one peak for resonant excitation to the detuned spectrum with at least three peaks clearly visible. This opposite behavior upon detuning of both participant spectra (in Figs. 2 and 4) was also reported very recently [14]. (Actually, we have become aware of these experimental observations only when the present manuscript was almost finished, i.e., after all our calculations had been completed.) Note that in both cases the peaks in the low-resolution spectra (left hand panels) seem to shift down in energy (from the top panel down) by less than required by the energy conservation condition in Eq. (35). However, this is only a consequence of the low radiation resolution: the peaks in the high-resolution spectra (right hand panels) are shifted by the expected amounts. Of course, the overall intensity of the spectra drops significantly when the radiation is detuned from the resonant conditions.

For the understanding of the features described in the preceding paragraph the time-dependent picture of the coherent process is particularly useful. For radiation frequencies out of tune with any resonant excitation the peaks are still expected for energies $\mathcal{E}=\mathcal{E}_{n'}^{\rm peak}(\omega_L)$ given in Eq. (35). For these energies, however, the condition of Eq. (36) can never be met. Consequently, the integrand in the time integration oscillates rapidly, the overall intensity becomes relatively small and, most importantly, the main contribution to the spectra comes from the wave packet at the *initial* stages of its time evolution due to the effects described around Eqs. (23) and (24). This explains nicely the observed evolution of the spectra across the panels in Figs. 2 and 4 if we realize that the initial wave packet is the vibrational ground state wave function of the electronic ground state potential $V_g(r)$. The potential $V_f(r)$ for the final ionic state $N_2^+[3\sigma_g^{-1}](X\ ^2\Sigma_g^+)$, appropriate to Fig. 2, is very similar to the ground state potential $V_g(r)$ of N_2; so the initial wave packet has a large overlap with the ground state wave function $(n'=0)$ of $V_f(r)$ and is almost orthogonal to all its excited vibrational $(n' \neq 0)$ wave functions. Therefore the detuned spectrum in Fig. 2 is dominated by one peak. In Fig. 4 the situation is reversed: the ground state potential $V_g(r)$ and the final ionic state potential $V_f(r)$ for $N_2^+[1\pi_u^{-1}](A\ ^2\Pi_u)$ are very different, so that the initial wave packet has a significant overlap with several final vibrational states n'. Consequently, several peaks are present in the detuned spectrum in Fig. 4. For the $N_2^+[1\pi_u^{-2},1\pi_g](D\ ^2\Pi_g)$ final configuration the fraction of molecular ions which undergo fragmentation increases as the radiation frequency is lowered below the lowest vibrational resonance of the core-excited state, and the electron spectra in the lowest panels of Fig. 6 become almost symmetric. This is expected in the reflection approximation for a nearly symmetric initial wave packet.

In general, the detuned spectra are essentially insensitive to the details of the time evolution of the wave packet along the core-excited state potential surface and are basically determined by the Franck-Condon factors between the initial wave packet and the vibrational wave functions of the final electronic configuration of the ion. This makes the Auger spectra similar in shape to the direct photoionization electron spectra at least in the approximation used in the present approach in which the dipole and the Auger transition operators were pulled out of the matrix elements. Selection rules, oscillator strengths, and the radiation polarization dependences may be entirely different for the two types of spectra. The initial and the final states for both types of processes are the same (unless the detailed selection rules would forbid that) so there might be an interference between them, particularly when both processes have similar oscillator strengths. This is not accounted for in the present approach.

As noted above, detuning and the consequent appearance of the spectrum can also be effectively achieved for a nominal radiation frequency significantly *larger* than that ω_L^v for which the Franck-Condon factor (involving the initial wave packet) is the largest. In such cases the components of the wave packet which contribute to the formation of the spectra for the longest time are again effectively suppressed due to their negligible overlap with the initial wave packet, and the role of the off-resonant components is relatively enhanced.

It is not our primary goal in this work to make a detailed comparison of the calculated and the experimental electron spectra; rather, we aim at a detailed understanding at a qualitative level of their evolution as the radiation frequency and bandwidth are varied. Still, some comparisons with the experimental spectra can be made and some comments to this effect were made earlier where appropriate. For N_2, the participant electron spectra were measured by Neeb *et al.* [15] using x-ray radiation with 0.1 eV bandwidth (i.e., between our 0.05 and 0.2 eV) tuned, in the nomenclature of the present paper, to $v \gtrsim 0$, $v \gtrsim 1$, $v \approx 2.5$, and $v \approx 3.5$. Our spectra in the left hand panels of Figs. 1 and 3 have all the characteristics seen in the experimental spectra in Fig. 4 of Ref. [15]. Similarly, a close correspondence can be seen between our spectra in Fig. 1 and the resonant $v=0$, 1, and 2 experimental spectra in Fig. 7 of Ref. [14] obtained for a radiation

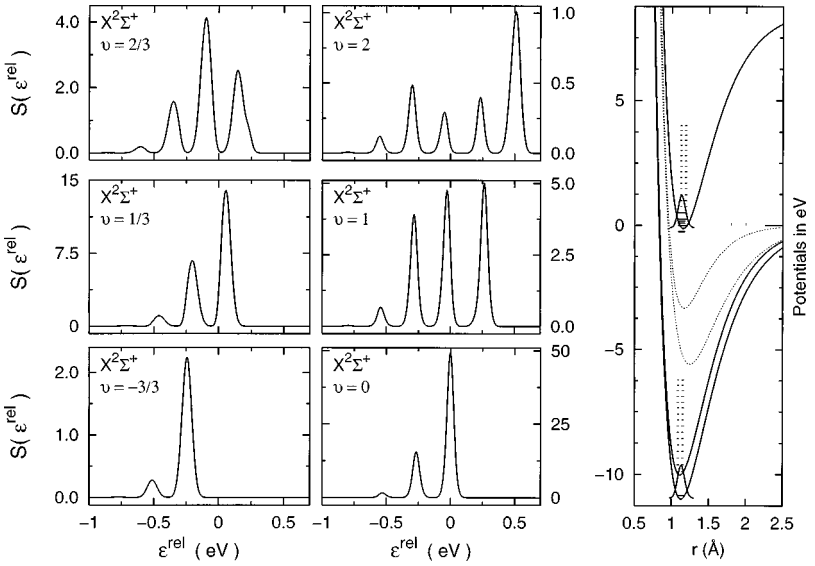

FIG. 7. Auger electron spectra for participant decay of the CO C 1s–hole excited state to the $[5\sigma^{-1}](X\ ^2\Sigma^+)$ state of the CO^+ ion for the monochromator resolution with FWHM $\Gamma_L=87$ meV and the core-excited state lifetime width $\Gamma=97$ meV. The nominal frequency of the exciting radiation is identified through υ, and the panel containing the potential energy curves, vibrational energy levels, and the initial wave packet is completely analogous to those in Figs. 1–6. Actual electron kinetic energy: $\mathcal{E}=\mathcal{E}^{\rm rel}+273.33$ eV [9].

bandwidth between 60 and 70 meV. Note that all experimental spectra are affected also by the finite electron detector resolution. The authors of both works actually provide an interpretation of their spectra in terms of the time-independent approach. It may be argued that even our resonant *spectator* spectra in Fig. 5 have minima and maxima at the same positions as the corresponding resonant spectra in Fig. 8 (for the electron kinetic energy above 375 eV) of Ref. [14]. However, comparison must be made very carefully because several spectator decay channels may overlap in the experimental spectra. Certainly, the vibrational structure of the final $D\ ^2\Pi_g$ ionic configuration (the ''fringes'' in Fig. 5) should not be resolved once the electron detector resolution is factored in, contrary to what the *theoretical* curves in Fig. 8 of Ref. [14] seem to indicate.

C. Results for the carbon monoxide molecule (CO)

In this subsection we present the calculated electron spectra resulting from C $1s\rightarrow\pi^*$ core hole primary excitation. More experimental spectra exist for this system than for N_2 both for low [15] and high x-ray and electron detector resolution; the latter for resonant primary excitations [9,13] and for the excitation detuned below [12] $\upsilon=0$. The work in Ref. [13] stands out not only because spectator spectra were measured in it as well, but also because the spectra have been theoretically calculated using a time-independent approach with an input for electronic states, potential curves, and all matrix elements evaluated by valence configuration interaction (VCI) calculations. Such an approach is very valuable for the spectator region of the decay spectrum in which many final ionic configurations overlap and their relative intensities are not *a priori* known.

We consider here only the participant Auger decays: the electron spectra in Figs. 7–9 correspond, respectively, to $CO^+[5\sigma^{-1}](X\ ^2\Sigma^+)$, $CO^+[4\sigma^{-1}](B\ ^2\Sigma^+)$, and $CO^+[1\pi^{-1}](A\ ^2\Pi)$, final electronic configurations of the CO^+ ion. Parameters of all the configurations are given in Table I. Following Ref. [9] we choose the core-excited state lifetime parameter $\Gamma=97$ meV and do the calculations for one only x-ray FWHM bandwidth $\Gamma_L=87$ meV. As for N_2, each figure contains a panel depicting the potential energy curves, initial wave packets, vibrational levels, primary ex-

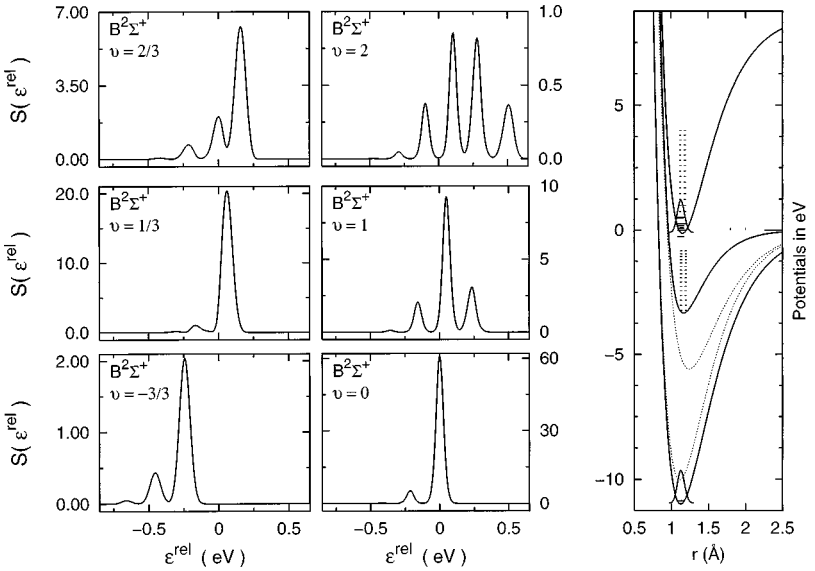

FIG. 8. The same as in Fig. 7 but for the spectator decay to state $[4\sigma^{-1}](B\ ^2\Sigma^+)$ of the CO^+ ion. Actual electron kinetic energy: $\mathcal{E}=\mathcal{E}^{\rm rel}+267.67$ eV [9].

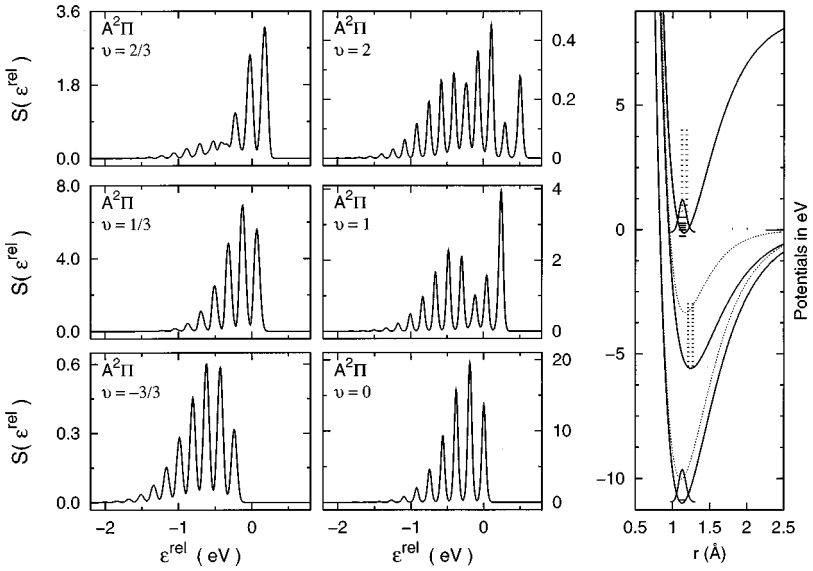

FIG. 9. The same as in Fig. 7 but for the spectator decay to state $[1\pi^{-1}](A\ ^2\Pi)$ of the CO^+ ion. Actual electron kinetic energy: $\mathcal{E} = \mathcal{E}^{\rm rel} + 270.81$ eV [9].

citation energies, and the vertical bars representing the lifetime parameter Γ, and the x-ray bandwidth Γ_L. The right hand panels show the spectra following resonant primary excitations to the $\upsilon = 0$ ($\hbar\omega_L^{\rm rel} = 0$), $\upsilon = 1$ ($\hbar\omega_L^{\rm rel} = 254.53$ meV), and $\upsilon = 2$ ($\hbar\omega_L^{\rm rel} = 505.29$ meV) vibrational levels of the core-excited state of CO. The lowest left hand panel corresponds to the spectrum obtained for the primary excitation detuned *below* the $\upsilon = 0$ excitation by the energy equal to $\hbar\omega_L^{\rm rel} = -254.53$ meV. The middle and the upper panels, respectively, are for the primary excitation tuned above the $\upsilon = 0$ level by one-third ($\hbar\omega_L^{\rm rel} = 84.83$ meV) and two-thirds ($\hbar\omega_L^{\rm rel} = 169.70$ meV) of the energy distance to the $\upsilon = 1$ level. The actual nominal photon energies can be obtained by adding [9] $T_{00} = 287.41$ eV to the values given above (recall that T_{00} does not affect the shape of the spectra).

For the C 1*s* resonance of CO, the core-excited state potential $V_d(r)$ is more similar to the ground state potential $V_g(r)$ (their frequency parameters and bond lengths differ by 4% and 2%, respectively) than for N_2 (with respective differences of 20% and 6%). Consequently, the x-ray absorption is dominated by the $\upsilon = 0$ peak which is about five times higher than the one corresponding to the $\upsilon = 1$ vibrational state of the core-excited state. One may therefore expect that the time evolution of the wave packet plays a relatively smaller role for CO than it does for N_2. Indeed, the shape of the spectra in the $\upsilon = 0$ panels is quite similar to that in the $\upsilon = -3/3$ panels in Figs. 7–9. The differences are significant enough to be observed experimentally [12] and will be discussed below.

Among the final states, the ionic ground state $CO^+[5\sigma^{-1}](X\ ^2\Sigma^+)$ has the frequency and the equilibrium bond length even closer to those of the neutral ground state than the core-excited state potential has (the respective differences are 2% and 1%). Consequently, the effects of detuning from the $\upsilon = 0$ resonant excitation to $\upsilon = -3/3$ below it, although small, are quite obvious in Fig. 7: the spectrum ''collapses'' from three peaks in the resonant $\upsilon = 0$ case to two only for the detuned one. This collapse of vibrational structure for CO is, indeed, observed and qualitatively explained using arguments based on the effective time over which the wave packet is allowed to evolve [12].

For the $CO^+[4\sigma^{-1}](B\ ^2\Sigma^+)$ final state the reverse effect is observed in Fig. 8: the resonant $\upsilon = 0$ spectrum is dominated by the $0 \searrow 0'$ peak accompanied by a small $0 \searrow 1'$ peak while the spectrum for off-resonance $\upsilon = -3/3$ excitation has two obvious peaks corresponding to the $n' = 0', 1'$ final vibrational states with the third, $n' = 2'$, peak also visible. This is also observed in Ref. [12] but the qualitative explanation provided there, based solely on the differences among the equilibrium bond lengths, seems to be oversimplified. Indeed, the difference between the equilibrium bond lengths between the initial and the final state potentials (3.5%) is larger than the difference between the equilibrium bond lengths of $V_d(r)$ and $V_f(r)$ (1.4%). But at least equally important for the presence of the three peaks in the detuned spectrum is the fact that the final state potential frequency parameter is about 20% smaller than that for the initial ground state $V_g(r)$. A delicate balance between the parameters plays a role here because $V_d(r)$ and $V_f(r)$ have also very different (about 17%) frequency parameters. This is why the evolution of the spectra from $\upsilon = 0$ through $\upsilon = 1$ to $\upsilon = 2$ excitations in Fig. 8 is so different than that observed in Fig. 3 for N_2. In fact, the qualitative explanation provided in Ref.[12] seems more appropriate to account for the evolution of the spectra observed for N_2 in Figs. 3 and 4 than for those in Fig. 8 for CO.

The final state $CO^+[1\pi^{-1}](A\ ^2\Pi)$ is very different from the previous two, because both its frequency parameter and equilibrium bond length are very different from those for both $V_g(r)$ and $V_d(r)$ (over 25% smaller and over 8% longer, respectively, than those for both these potentials). Consequently, the spectra in Fig. 9 exhibit an increasing number of peaks not only as the radiation is resonantly tuned to $\upsilon = 0$ (9 peaks), $\upsilon = 1$ (11 peaks), and $\upsilon = 2$ (13 peaks); but also when detuned below $\upsilon = 0$ (10 peaks in $\upsilon = -3/3$ panel). For resonant excitation the component of the time-dependent wave packet which contributes for the longest time to the formation of the spectra has increasingly more nodes for higher excitations, so it overlaps with larger numbers of the final vibrational levels n', and larger numbers of peaks are observed for more energetic excitations. For detuned excita-

tion, the number of peaks is also larger than that for the $v=0$ resonant excitation because the ground state potential $V_g(r)$ differs from the final potential $V_f(r)$ more than $V_d(r)$ does.

IV. CONCLUSIONS

In this paper we have developed an explicitly time-dependent theory for one-step resonant excitation-deexcitation processes of core electron states in diatomic molecules, paying special attention to its conceptual simplicity and interpretational appeal. We use the ensuing formalism to calculate the Auger electron decay spectra for the model diatomic systems N_2 and CO, and to demonstrate important features following from such processes. In particular, we stress the influence of the effective time over which the spectrum is formed during the evolution of the time-dependent wave packet which describes the relative motion of two atoms in the core-excited molecule. We show that when the exciting radiation is in tune with the resonant excitations to the vibrational levels of the core-excited molecule, the long-time behavior of the evolving wave packet—limited only by the lifetime of the core hole—determines the shape of the spectrum in which both the vibrational structure of the final molecular ion and the nodal structure of the vibrational wave functions of the core-excited state are reflected. On the other hand, if the exciting radiation is detuned from the resonance, only the initial time evolution of the wave packet is crucial; this makes the spectra less sensitive to the intramolecular binding in the core-excited intermediate state. The influence of the excitation bandwidth on the appearance of the spectra, i.e., the Auger resonant Raman effect, is explicitly demonstrated for N_2. Decay spectra calculated for various final states of N_2 and CO clearly exhibit the influences of the positions and shapes of the relevant potential curves. The calculated spectra are in good overall agreement with the available experimental spectra although no attempt was made at detailed fits.

ACKNOWLEDGMENTS

We thank Wilfried Wurth for helpful discussions, for providing us with many experimental and interpretational insights, and for a critical reading of the manuscript. We are grateful to A. M. Bradshaw for a preprint of Ref. [14] prior to acceptance. Z.W.G. would like to thank his colleagues at the Physics Department of the Technical University of Munich for their hospitality during his visits there, and J.-P. de Villiers for writing the numerical code for the wave-packet propagation. This work was supported by a research grant from the Natural Sciences and Engineering Research Council (NSERC) of Canada, and by Grant No. SFB 338 of the Deutsche Forschungsgemeinschaft.

APPENDIX A

In order to make the formulas easier to read we denote by $A(t)$ the entire expression inside the curly brackets in Eq. (18). Further, denoting

$$x^{\pm}=(E_{\rm in}\pm\hbar\omega-E_{\chi}^{f}-\mathcal{E}_{\mathbf{k}})/\hbar, \tag{A1a}$$

$$z^{\pm}=(E_{\rm in}\pm\hbar\omega+i\Gamma/2)/\hbar, \tag{A1b}$$

$$f(t'')=\langle\varphi_{\chi}^{f}|W_{f\mathbf{k}}^{\dagger}|\phi_d(t'')\rangle, \tag{A1c}$$

we get

$$A(t)=\int_0^t dt'\exp(ix^{+}t')\int_0^{t'}dt''\exp(iz^{+}t'')f(t'') + \int_0^t dt'\exp(ix^{-}t')\int_0^{t'}dt''\exp(iz^{-}t'')f(t''). \tag{A2}$$

Note that $z^{\pm}$ have positive imaginary parts, so the exponential factors containing $z^{\pm}$ vanish for $t''\to\infty$. Reversing the order of both integrations

$$\int_0^t dt'\int_0^{t'}dt''\cdots=\int_0^t dt''\int_{t''}^t dt'\cdots \tag{A3}$$

allows us to integrate over t' explicitly. The result (in which t'' is renamed to t') is

$$A(t)=\int_0^t dt' f(t')\exp(iz^{+}t')\frac{\exp(ix^{+}t)-\exp(ix^{+}t')}{ix^{+}} + \int_0^t dt' f(t')\exp(iz^{-}t')\frac{\exp(ix^{-}t)-\exp(ix^{-}t')}{ix^{-}}. \tag{A4}$$

We also need the time derivative of $A(t)$ which we compute from Eq. (A2):

$$\dot{A}(t)=\exp(ix^{+}t)\int_0^t dt'' f(t'')\exp(iz^{+}t'') + \exp(ix^{-}t)\int_0^t dt'' f(t'')\exp(iz^{-}t''). \tag{A5}$$

The time derivative of $|A(t)|^2$ can now be calculated as $A^*\dot{A}+A\dot{A}^*$ using Eqs. (A4) and (A5). The result is a lengthy expression containing a term involving x^{+} and z^{+}, an identical term but with x^{-} and z^{-}, and a ''mixed'' term containing both superscripts, $+$ and $-$. In the long-time limit, $t\to\infty$, the dominant contribution comes from the first two terms; so we consider them only and ignore the mixed term. Both remaining terms have the same structure so we drop the superscripts in what follows. We get

$$\frac{d}{dt}|A(t)|^2=\int_0^t dt'\int_0^t dt'' f^*(t')f(t'')\exp(-iz^*t') \times\exp(izt'') \times\frac{\exp[ix(t-t')]-\exp[-ix(t-t'')]}{ix}, \tag{A6}$$

which should be understood in such a way that $d|A|^2/dt$ is a sum of two terms like the one above, one in which x and z

have the superscript + and the one in which the superscript is −. Note that the exponential factors containing z result in a factor $\exp[-\eta(t'+t'')/2]$; so in the limit $t \gg \eta^{-1}$ the main contributions to both integrations are due to $t', t'' \ll \eta^{-1} \ll t$. Therefore t' and t'' may be ignored in comparison with t in the exponential functions containing x. The result is

$$\frac{d}{dt}|A(t)|^2 \approx \frac{2\,\sin(xt)}{x}\left|\int_0^t dt' f(t')\exp(izt')\right|^2. \quad \text{(A7)}$$

Taking the long-time limit needed in Eq. (16) we get, after restoring the ± superscripts,

$$\lim_{t\to\infty}\frac{d}{dt}|A(t)|^2 = 2\pi\delta(x^+)\left|\int_0^\infty dt' f(t')\exp(izt')\right|^2 + 2\pi\delta(x^-)\left|\int_0^\infty dt' f(t')\exp(izt')\right|^2, \quad \text{(A8)}$$

where the well-known long-time limit $\sin(xt)/x \to \pi\delta(x)$ was used. After physical quantities are restored according to Eqs. (A1) both δ's become the energy conservation δ functions: $\delta(E_{\rm in} \pm \hbar\omega - E^f_\chi - \mathcal{E}_{\boldsymbol{k}})$. Because $E_{\rm in}$ is the lowest energy possible for the system, only the term with $+\hbar\omega$ survives and $d\dot{P}_{\chi,f\boldsymbol{k}}(\omega)$ in Eq. (16) becomes proportional to $\delta(E_{\rm in}+\hbar\omega - E^f_\chi - \mathcal{E}_{\boldsymbol{k}})$. Therefore the initial energy of the nuclear motion in the molecule in its electronic ground state plus the energy of the absorbed photon is shared between the final energy of the nuclear motion in the molecular ion and the kinetic energy of the escaping electron.

APPENDIX B

We outline here the derivation of Eqs. (30) from Eq. (22). The initial condition for the time evolution of $\phi_d(\boldsymbol{r},t)$ is the *spherically symmetric* ground state wave function $\psi_{\rm in}(\boldsymbol{r})$ of the ground state potential $V_g(r)$. It evolves in time along the *spherically symmetric* potential $V_d(r)$. Therefore the time-dependent wave packet $\phi_d(\boldsymbol{r},t)$ remains spherically symmetric. In other words, the spherical harmonics expansions of the initial and time-dependent wave packets involve only the lowest order $l=m=0$ term:

$$\psi_{\rm in}(\boldsymbol{r}) = Y_{00}(\hat{\boldsymbol{r}})\frac{u_{\rm in}(r)}{r}, \quad \text{(B1a)}$$

$$\phi_d(\boldsymbol{r},t) = Y_{00}(\hat{\boldsymbol{r}})\frac{u_d(r,t)}{r}, \quad \text{(B1b)}$$

$$u_d(r,t=0) = u_{\rm in}(r). \quad \text{(B1c)}$$

Here, $Y_{00}(\hat{\boldsymbol{r}}) = 1/\sqrt{4\pi}$, $u_{\rm in}(r)$ is a normalized ground state wave function solution of the *one-dimensional* Schrödinger equation (32) involving the potential $V_g(r)$. It is the initial condition for $u_d(r,t)$ which satisfies the *one-dimensional* time-dependent Schrödinger equation (31) involving $V_d(r)$.

To deal with the eigenfunctions of H_f, i.e., $\varphi^f_\chi(\boldsymbol{r})$, we must treat the localized and the extended states separately.

For the localized eigenstates the appropriate quantum numbers are $\chi = (n',l,m)$ so

$$\varphi^f_\chi(\boldsymbol{r}) \equiv \varphi^f_{n',l,m}(\boldsymbol{r}) = Y_{lm}(\hat{\boldsymbol{r}})\frac{u^f_{n',l}(r)}{r}, \quad \text{(B2)}$$

where $u^f_{n',l}(r)$ is the n'th eigenfunction of the one-dimensional Schrödinger equation containing $V_f(r)$ and the l-dependent centrifugal potential. When the overlap with the spherically symmetric time-dependent wave packet is computed, one gets

$$\langle \varphi^f_{n',l,m}|\phi_d(t)\rangle = \delta_{l,0}\delta_{m,0}\langle u^f_{n'}|u_d(t)\rangle, \quad \text{(B3)}$$

where we write $u^f_{n'}$ rather than $u^f_{n',0}$ for the n'th discrete state eigenfunction of a one-dimensional Schrödinger equation (33) containing $V_f(r)$. Similarly, the corresponding energy eigenvalue will be denoted $E^f_{n'}$ rather than $E^f_{n',0}$. Inserting Eq. (B3) into Eq. (22) we obtain Eq. (30a) for the ''localized'' contribution to the cross section.

For the extended states the appropriate wave function $\varphi^f_\chi(\boldsymbol{r})$ is such an eigenfunction of H_f, $\varphi^{f(-)}(\boldsymbol{r},\boldsymbol{q})$, which corresponds to the energy eigenvalue $E(q) = \hbar^2 q^2/2\mu$ (with μ being the effective mass for the relative motion of both constituents of the molecule) and which for $r\to\infty$ consists of a plane wave $\propto \exp(i\boldsymbol{q}\cdot\boldsymbol{r})$ and the *ingoing* spherical wave $\propto \exp(-iqr)/r$. The *summation* over χ in Eq. (22) for this part of the spectrum can, in the infinite volume limit $V\to\infty$, be replaced with the *integration* over $d^3\boldsymbol{q}$, provided the necessary density of states factor $V/(2\pi)^3$ gets incorporated into the definition of the extended state wave functions

$$\left(\frac{V}{(2\pi)^3}\right)^{1/2}\varphi^f_\chi(\boldsymbol{r}) \to \varphi^{f(-)}(\boldsymbol{r},\boldsymbol{q}), \quad \text{(B4)}$$

which now are normalized to $\delta^{(3)}(\boldsymbol{q}-\boldsymbol{q}')$. The partial wave expansion of this function is

$$\varphi^{f(-)}(\boldsymbol{r},\boldsymbol{q}) = \sum_{l=0}^{\infty}\sum_{m=-l}^{m=l} i^l \exp[-i\delta^f_l(q)] \times \frac{u^f_l(r,q)}{qr} Y^*_{lm}(\hat{\boldsymbol{q}})Y_{lm}(\hat{\boldsymbol{r}}), \quad \text{(B5)}$$

where $u^f_l(r,q)$ is an extended state eigenfunction of the one-dimensional Schrödinger equation containing $V_f(r)$ and the l-dependent centrifugal potential. The wave function corresponds to the energy eigenvalue $E(q)$ and satisfies the following boundary condition for $r\to\infty$:

$$u^f_l(r,q) \to \sqrt{\frac{2}{\pi}}\sin[qr - l\pi/2 + \delta^f_l(q)], \quad \text{(B6)}$$

where $\delta^f_l(q)$ is a partial wave phase shift which will not be needed in what follows. When the matrix element with the spherically symmetric time-dependent wave packet $\phi_d(\boldsymbol{r},t)$, given in Eq. (B1b), is computed then only the $l=m=0$ term survives:

$$\langle \varphi^{f(-)}(\boldsymbol{q})|\phi_d(t)\rangle = Y_{00}(\hat{\boldsymbol{q}})\frac{\exp[i\delta_0^f(q)]}{q}\langle u^f(q)|u_d(t)\rangle. \tag{B7}$$

We write here $u^f(q)$ rather than $u_0^f(q)$ for the extended state eigenfunction corresponding to the energy eigenvalue $E(q)$ of a one-dimensional Schrödinger equation containing $V_f(r)$. The phase factor disappears and Y_{00}/q gets canceled out when the modulus square is taken, $d^3\boldsymbol{q}$ is replaced with $q^2dqd\Omega$, and the angular integration is made. The result is Eq. (30b) for the ''extended'' contribution to the cross section.

APPENDIX C

The initial wave packet $u_{\rm in}(r)$ is a ground state solution of the Schrödinger equation (31). For the Morse potential in Eq. (40) it reads

$$u_{\rm in}(r) = \sqrt{\gamma_g}\frac{(2\sigma_g)^{\sigma_g-1/2}}{\sqrt{\Gamma(2\sigma_g-1)}}\exp(-\sigma_g e^{-\gamma_g(r-r_g)}) \times\exp[-\gamma_g(\sigma_g-1/2)(r-r_g)], \tag{C1}$$

where $\Gamma(x)$ is Euler's gamma function [43] and σ_g is defined in Eq. (44) for $\alpha=g$. The time-dependent Schrödinger equation (31) is then solved numerically using the spectral method of Kosloff and Kosloff [44]. The solution may be done in advance and the result, the real and the imaginary parts of the wave packet at predetermined values of r and t, may be stored in a file for further use. If Heller's semiclassical method [34] of solution of the time-dependent Schrödinger is going to be used then the initial wave packet (C1) should be approximated by a Gaussian

$$u_{\rm in}(r)\approx\sqrt{\gamma_g}(\sigma_g/\pi)^{1/4}\exp[-\sigma_g\gamma_g^2(r-r_g)^2/2], \tag{C2}$$

which is a good approximation to Eq. (C1) for $\sigma_g\gg1$. For the Morse potential representation of $V_d(r)$ Heller's solution can be obtained in the analytic form [32,33]. It was checked that such a solution approximates the exact one quite well, but in this work we use the exact numerical time evolution of the wave packet starting from the initial condition (C1).

For $V_f(r)$ given by the Morse potential in Eq. (39) it is convenient to introduce an auxiliary variable $s=\exp[-\gamma_f(r-r_f)]$. Then, the bound state wave functions $u_{n'}^f(r)$ of the Schrödinger equation (33) are

$$u_{n'}^f(r) = \sqrt{\gamma_f}\left(\frac{n'!(2\sigma_f-2n'-1)}{\Gamma(2\sigma_f-n')}\right)^{1/2}(2\sigma_f s)^{\sigma_f-n'-1/2} \times e^{-\sigma_f s}L_{n'}^{(2\sigma_f-2n'-1)}(2\sigma_f s), \tag{C3}$$

where $L_n^{(\eta)}(z)$ denotes the generalized Laguerre polynomial [43] of degree n and σ_f is defined in Eq. (44) for $\alpha=f$. For $n'=0'$ (the ground state) the above function reduces to the form given in Eq. (C1) with indices g replaced with f. The energy eigenvalues [measured on the energy scale defined in Eq. (28)] corresponding to $u_{n'}(r)$ are given by

$$E_{n'}^f = -\frac{\hbar^2\gamma_f^2}{2\mu}(\sigma_f-n'-1/2)^2. \tag{C4}$$

An analytic expression exists for the wave function $u^f(r,q)$ for an extended state corresponding to the energy $E(q)=\hbar^2q^2/2\mu$ for the Morse potential $V_f(r)$. Such an expression is, however, numerically unstable rendering it practically useless in our work. Very accurate results are obtained using the WKB approximation. In order to satisfy the boundary condition which radial functions must satisfy at $r=0$ one should add a term $\hbar^2/8\mu r^2$ to $V_f(r)$ to get the s-wave radial wave function in the WKB approximation [45]. In practice, however, this term may be ignored because of its negligible effect. Therefore the WKB wave function satisfying the boundary condition given in Eq. (34) reads

$$u^f(r,q) = \left|\frac{4E(q)g(r,q)}{E(q)-V_f(r)}\right|^{1/4}\mathrm{Ai}(-g(r,q)), \tag{C5}$$

where $\mathrm{Ai}(z)$ is the Airy function [43] and

$$g(r,q) = \mathrm{sgn}[r-r_c(q)] \times\left|\frac{3}{2\hbar}\int_{r_c(q)}^{r}dr'\sqrt{2\mu|E(q)-V_f(r)|}\right|^{2/3}. \tag{C6}$$

Here, $r_c(q)$ is the classical turning point at which the integrand in Eq. (C6) vanishes. A nice feature of the Morse potential form of $V_f(r)$ is that an algebraic expression exists for $g(r,q)$. Introducing the dimensionless energy $\epsilon=E(q)/V_f$ and using the auxiliary variable $s=\exp[-\gamma_f(r-r_f)]$ already introduced above Eq. (C3) we get, respectively, for $r<r_c(q)$ (in the classically forbidden region) and for $r>r_c(q)$ (classically allowed region),

$$g_l(r,q) = -\left\{-\frac{3}{2}\sigma_f\left[\sqrt{\epsilon}\arccos\left(\frac{\epsilon+s}{s\sqrt{1+\epsilon}}\right) +\ln\left(\frac{s-1+\sqrt{s^2-2s-\epsilon}}{\sqrt{1+\epsilon}}\right) -\sqrt{s^2-2s-\epsilon}\right]\right\}^{2/3}, \tag{C7a}$$

$$g_r(r,q) = \left\{\frac{3}{2}\sigma_f\left[\arccos\left(\frac{s-1}{\sqrt{1+\epsilon}}\right) +\sqrt{\epsilon}\ln\left(\frac{\epsilon+s+\sqrt{\epsilon(\epsilon+2s-s^2)}}{s\sqrt{1+\epsilon}}\right) -\sqrt{\epsilon+2s-s^2}\right]\right\}^{2/3}, \tag{C7b}$$

where the subscripts l and r refer to regions $r<r_c(q)$ and $r>r_c(q)$, respectively.

[1] *Resonant Anomalous X-ray Scattering: Theory and Applications*, edited by G. Materlik, C. Sparks, and K. Fisher (North-Holland, Amsterdam, 1994).
[2] T. Åberg and B. Crasemann, in Ref. [1], p. 431, and references therein.
[3] P. L. Cowan, in Ref. [1], p. 449.
[4] F. Gel'mukhanov and H. Ågren, Phys. Lett. A **193**, 375 (1994).
[5] G. B. Armen and H. Wang, Phys. Rev. A **51**, 1241 (1995).
[6] E. Kukk, S. Aksela, and H. Aksela, Phys. Rev. A **53**, 3271 (1996).
[7] T. D. Thomas and T. X. Caroli, Chem. Phys. Lett. **185**, 31 (1991).
[8] M. Neeb, J.-E. Rubensson, M. Biermann, W. Eberhardt, K. J. Randall, J. Feldhaus, A. L. D. Kilcoyne, A. M. Bradshaw, Z. Xu, P. D. Johnson, and Y. Ma, Chem. Phys. Lett. **212**, 205 (1993).
[9] S. J. Osborne, A. Ausmees, S. Svensson, A. Kivimäki, O.-P. Sairanen, A. Naves de Brito, H. Aksela, and S. Aksela, J. Chem. Phys. **102**, 7317 (1995).
[10] P. Skytt, P. Glans, K. Gunnelin, J. Guo, and J. Nordgren, Phys. Rev. A **55**, 146 (1997).
[11] N. M. Piancastelli, M. N. Neeb, A. Kivimäki, B. Kempgens, H. M. Köppe, K. Maier, and A. M. Bradshaw, Phys. Rev. Lett. **77**, 4302 (1996).
[12] S. Sundin, F. Kh. Gel'mukhanov, H. Ågren, S. J. Osborne, A. Kikas, O. Björnholm, A. Ausmees, and S. Svensson, Phys. Rev. Lett. **79**, 1451 (1997).
[13] M. N. Piancastelli, M. Neeb, A. Kivimäki, B. Kempgens, H. M. Köppe, K. Maier, A. M. Bradshaw, and R. F. Fink, J. Phys. B **30**, 5677 (1997).
[14] N. M. Piancastelli, A. Kivimäki, B. Kempgens, M. Neeb, K. Maier, U. Hergenhahn, A. Rüdel, and A. M. Bradshaw, J. Electron Spectrosc. Relat. Phenom. (to be published).
[15] M. Neeb, J.-E. Rubensson, M. Biermann, and W. Eberhardt, J. Electron Spectrosc. Relat. Phenom. **67**, 261 (1994).
[16] A. Kivimäki, B. Kempgens, N. M. Piancastelli, M. Neeb, K. Maier, A. Rüdel, U. Hergenhahn, and A. M. Bradshaw, J. Electron Spectrosc. Relat. Phenom. (to be published).
[17] E. Kukk, H. Aksela, S. Aksela, F. Gel'mukhanov, H. Ågren, and S. Svensson, Phys. Rev. Lett. **76**, 3100 (1996).
[18] O. Björneholm, S. Sundin, S. Svensson, R. R. T. Marinho, A. Naves de Brito, F. Gel'mukhanov, and H. Ågren, Phys. Rev. Lett. **79**, 3150 (1997).
[19] C. Keller, M. Stichler, G. Comelli, F. Esch, S. Lizzit, W. Wurth, and D. Menzel, Phys. Rev. Lett. **80**, 1774 (1998); C. Keller, M. Stichler, G. Comelli, F. Esch, S. Lizzit, D. Menzel, and W. Wurth, J. Electron Spectrosc. Relat. Phenom. (to be published).
[20] T. Åberg, Phys. Scr. **21**, 495 (1980); **T41**, 71 (1992).
[21] F. Gel'mukhanov and H. Ågren, Phys. Rev. A **54**, 3960 (1996).
[22] F. Gel'mukhanov, T. Privalov, and H. Ågren, Phys. Rev. A **56**, 256 (1997).
[23] P. Skytt, P. Glans, J.-H. Guo, K. Gunnelin, C. Såthe, J. Nordgren, F. Kh. Gel'mukhanov, A. Cesar, and H. Ågren, Phys. Rev. Lett. **77**, 5035 (1996).
[24] A. Cesar, F. Gel'mukhanov, Y. Luo, H. Ågren, P. Skytt, P. Glans, J. Guo, K. Gunnelin, and J. Nordgren, J. Chem. Phys. **106**, 3439 (1997).
[25] F. Gel'mukhanov, T. Privalov, and H. Ågren, Zh. Éksp. Teor. Fiz. **112**, 37 (1997) [JETP **85**, 20 (1997)].
[26] L. S. Cederbaum and F. Tarantelli, J. Chem. Phys. **98**, 9691 (1993).
[27] E. Pahl, H.-D. Meyer, and L. S. Cederbaum, Z. Phys. D **38**, 215 (1996).
[28] F. Gel'mukhanov and H. Ågren, Phys. Rev. A **54**, 379 (1996).
[29] Z. W. Gortel, J.-P. de Villiers, Chem. Phys. Lett. **245**, 41 (1995).
[30] A. Naves de Brito, S. Svensson, S. J. Osborne, A. Ausmees, A. Kivimäki, O.-P. Sairanen, E. Nõmmiste, H. Aksela, S. Aksela, and L. J. Sæthre, J. Chem. Phys. **106**, 18 (1997).
[31] Z. W. Gortel, H. J. Kreuzer, P. Feulner, and D. Menzel, in *Desorption Induced by Electronic Transitions, DIET III*, edited by R. H. Stulen and M. L. Knotek, Springer Series in Surface Sciences Vol. 1 (Springer-Verlag, Berlin, 1988), p. 173; Z. W. Gortel, R. Teshima, and H. J. Kreuzer, Phys. Rev. B **37**, 3183 (1988).
[32] Z. W. Gortel and A. Wierzbicki, Phys. Rev. B **43**, 7487 (1991).
[33] Z. W. Gortel and R. Teshima, Phys. Rev. B **47**, 9825 (1993).
[34] E. J. Heller, J. Chem. Phys. **62**, 1544 (1975).
[35] Soo-Y. Lee and E. J. Heller, J. Chem. Phys. **71**, 4777 (1979).
[36] R. Murphy, I.-W. Lyo, and W. Eberhardt, J. Chem. Phys. **88**, 6078 (1988).
[37] F. K. Gel'mukhanov, L. N. Mazalov, and A. V. Kondratenko, Chem. Phys. Lett. **46**, 133 (1977).
[38] F. Gel'mukhanov, H. Ågren, S. Svensson, H. Aksela, and S. Aksela, Phys. Rev. A **53**, 1379 (1996).
[39] K. P. Huber and G. Herzberg, *Molecular Spectra and Molecular Structure, Vol. 4: Constants of Diatomic Molecules* (Van Nostrand Reinhold, New York, 1950).
[40] C. T. Chen, Y. Ma, and F. Sette, Phys. Rev. A **40**, 6737 (1989); C. T. Chen (private communication).
[41] W. Ebarhardt, E. W. Plummer, I.-W. Lyo, R. Murphy, R. Carr, and W. K. Ford, J. Phys. (Paris), Colloq. **48**, C9-679 (1987).
[42] T. Namioka, K. Yoshino, and Y. Tanaka, J. Chem. Phys. **39**, 2629 (1963).
[43] *Handbook of Mathematical Functions*, edited by M. Abramowitz and I. A. Stegun, Natl. Bur. Stand. Appl. Math. Ser. No. 55 (U.S. GPO, Washington, 1965).
[44] D. Kosloff and R. A. Kosloff, J. Comput. Phys. **52**, 35 (1983).
[45] C. J. Joachain, *Quantum Collision Theory* (North-Holland, Amsterdam, 1983).
[46] D. W. Turner, C. Baker, A. D. Baker, and C. R. Brundle, *Molecular Photoelectron Spectroscopy* (Wiley, New York, 1970).
[47] M. Okuda and N. Jonathan, J. Electron Spectrosc. Relat. Phenom. **3**, 19 (1974).
[48] P. Baltzer, M. Larsson, L. Karlsson, B. Wannberg, and M. Carlsson Göthe, Phys. Rev. A **46**, 5545 (1992).